Studies with Improved Renormalization Group Techniques

by

Gregory James Petropoulos

B.S., University of Connecticut, 2010

M.S., University of Colorado, 2013

A thesis submitted to the

Faculty of the Graduate School of the

University of Colorado in partial fulfillment

of the requirements for the degree of

Doctor of Philosophy

Department of Physics

2014

This thesis entitled:
Studies with Improved Renormalization Group Techniques
written by Gregory James Petropoulos
has been approved for the Department of Physics

_____

Anna Hasenfratz

_____

Prof. Thomas DeGrande

_____

Prof. Ethan Neil

_____

Prof. Senarath de Alwis

_____

Prof. Thomas A. Manteuffel

Date _____

The final copy of this thesis has been examined by the signatories, and we find that both the content and the form meet acceptable presentation standards of scholarly work in the above mentioned discipline.

Petropoulos, Gregory James (Ph.D., Physics)

Studies with Improved Renormalization Group Techniques

Thesis directed by Prof. Anna Hasenfratz

Dedication

Acknowledgements

Contents

Appendix

Tables

Table

Figures

Figure

Chapter 1

Introduction

1.1   Motivation

The standard model (SM) was recently completed with the discovery of the Higgs particle at the Large Hadron Collider (LHC) in Geneva. While the standard model doesn't predict any new fundamental particles we know that it is not the complete description of nature. It was hoped by many that the LHC would discover new particles in addition to the Higgs particle. Since these particles would not be part of the standard model they would necessitate new physics. Many beyond standard model (bsm) theories exist that predicted new particles and confirmation of one or more of these theories would usher in a new age of discovery at the energy frontier. This however has not come to pass, the Higgs arrived unaccompanied.

The Higgs particle in the standard model is an excitation of the Higgs field which itself is responsible for electroweak symmetry breaking (EWSB). EWSB explains how the $W^{\pm}$ and Z bosons acquire a mass that would otherwise be forbidden by electroweak unification. Additionally in the EWSB process the Higgs develops a vacuum expectation value (VEV). The standard model fermions couple to the VEV and allow them to acquire mass without violating local gauge invariance.

The Higgs field in the standard model is a scalar field. This leads to the hierarchy problem (also equivalent to the naturalness or fine tuning problem) as the Higgs mass will be dependant on the UV cutoff of the theory. If the standard model is the complete story and there is no new physics just above the electroweak scale then we expect the Higgs mass to be at the same order as the cutoff. The fact the Higgs mass is 126 GeV requires fine tuning in the electroweak sector to

cancel the UV divergences.

There have been many solutions proposed as an alternative to the Standard Model that don't require fine tuning. Super Symmetry (SUSY) is one such proposal that achieves cancellations by introducing a new symmetry between bosonic and fermionic fields. Since the bosons and fermions enter loop calculations with opposite signs there is no need for fine tuning. Currently SUSY is constrained by the Higgs mass and the fact we haven't seen any of the super partners of the standard model particles. Additionally most versions of SUSY that have not been ruled out replace the standard model hierarchy problem with a new 'little' hierarchy problem where fine tuning is still required but it is not as severe as it is in the standard model.

Another natural possibility is that EWSB is the result of new strong dynamics at the TeV scale. Under this prescription EWSB happens much like spontaneous chiral symmetry breaking in quantum chromodynamics (QCD). QCD is the only strongly coupled sector of the standard model and is responsible for the strong nuclear force. Theories of EWSB that rely on strong dynamics are generally called Technicolor models. Technicolor is also highly constrained by the Higgs mass, the top quark mass, and precision electroweak measurements that show the flavor changing neutral currents are highly suppressed.

It is natural to draw insights from the parallels of Technicolor and QCD or directly from perturbation theory, however such insights are not the full story. The strongly coupled nature of these theories demands that they are studied through fully nonperturbative means. Therefore, lattice gauge theory is the only controlled way to study these theories. Lattice QCD, the study of QCD on the lattice, has been extremely successfully in understanding QCD. In lattice gauge theory we discretized euclidean space time into a regular grid of sites connected by links. The Lagrangian describing the theory is also discretized in such a way that in the continuum limit the original theory is recovered. The continuum limit is the limit that the lattice is taken to be infinitely large and the sites are infinitesimally close together.

The ultimate goal of efforts in this field is to find a theory can explain electroweak symmetry breaking, as it is observed in nature, through new strong dynamics. Finding such a theory is highly

non trivial and a great deal of theoretical and computational effort has gone into looking for such a theory. The lattice community has set out to do this in a controlled way. Map out the space of all possible theories and see what we find. To date a lot of the focus of the lattice community has been on locating the conformal window and developing techniques to distinguish conformal from chiraly broken theories.

This thesis has two primary objectives. The first goal is a physics goal: map out the behavior of $SU(3)$ gauge theories with N_f fermions in the fundamental representation. For technical reasons we choose to study theories with 4, 8, 12, and 16 flavors. 4 and 16 flavor theories are already well understood so the focus of our work is on 8 and 12 flavor systems.

My second objective is to develop tools that make the first goal possible. Towards this end I introduce improvements to lattice step scaling calculation techniques. I explore how these techniques are different and how to implement them in a calculation. Finally these techniques are applicable to any lattice calculation and therefore will be of use to any lattice practitioner.

1.2   Organization

This thesis is organized into five chapters not including the introduction and conclusion. Briefly, I use chapter 2 to set the stage and chapter 3 to give a flavor for lattice calculations. Chapters 4-6 discuss my contributions, each chapter is its own calculation and reflects approximately a years worth of work.

I begin chapter 2 with a brief overview of the standard model giving the Higgs mechanism its own section due to its relevance for the remainder of the thesis. I then summarized flaws in our current understanding of the standard model with emphasis given to the hierarchy problem. Finally I discuss how a composite Higgs can resolve the hierarchy problem in a natural way. Because a composite Higgs arises from a strongly interacting quantum field theory we can not understand such a theory with the standard analytical tools. Fortunately there is a well developed nonperturbative appraoch, lattice gauge theory. I conclude the chapter with an overview of current lattice studies.

Chapter 3 provides the reader with a brief overview of lattice gauge theory. Like any mature

discipline, this topic is a subject of many books. My goal is not to cover this subject comprehensively; rather I want to provide the reader with a flavor of how a lattice calculation is performed and highlight areas that are useful in later sections.

Chapter 4 - 6 document the body of work that is this thesis. Chapter 4 concerns my early work using Monte Carlo Renormalization Group (MCRG) on SU(3) $N_f = 8$ and SU(3) $N_f = 12$ theories. In chapter 5 I introduce the gradient flow and how it can be used to calculate the renormalized beta function. I also use this chapter to discuss an optimization improvement that our group developed. Results for for SU(3) $N_f = 4$ and SU(3) $N_f = 12$ are given. Finally chapter 6 shows how the Wilson Flow can be used as an optimization step for MCRG. Results from SU(3) $N_f = 12$ are given.

In my concluding chapter I make some final remarks about interpreting our results. I will also summarize results from other methods that our group used to study this system. All of the methods our group has used to study there systems have converged to the same answer making a strong case.

1.3   Notation and Conventions

Unless otherwise noted these are the standard conventions used in this thesis. I use standard particle theory units of $\hbar = c = 1$. The four vector is given by Greek indices

$$x^\mu = \begin{pmatrix} x_0 \\ x_1 \\ x_2 \\ x_3 \end{pmatrix},$$
(1.1)

where x_0 is the temporal component t and the remaining three components are the spatial components of $\vec{x}$. For the metric I use the west coast convention for the metric

$$\eta_{\mu\nu} = \begin{pmatrix} 1 & 0 & 0 & 0 \\ 0 & -1 & 0 & 0 \\ 0 & 0 & -1 & 0 \\ 0 & 0 & 0 & -1 \end{pmatrix}. \tag{1.2}$$

Standard Einstein summation notation applies to contract indices.

I work in the chiral representation for the Dirac spin matrices γ^μ

$$\gamma^0 = \begin{pmatrix} 0 & I \\ I & 0 \end{pmatrix}, \quad \gamma^i = \begin{pmatrix} 0 & \sigma^i \\ -\sigma^i & 0 \end{pmatrix}, \tag{1.3}$$

where I is the 2×2 identity matrix and σ^i are the Pauli matrices:

$$I = \begin{pmatrix} 1 & 0 \\ 0 & 1 \end{pmatrix}, \quad \sigma^1 = \begin{pmatrix} 0 & 1 \\ 1 & 0 \end{pmatrix}, \quad \sigma^2 = \begin{pmatrix} 0 & -i \\ i & 0 \end{pmatrix}, \quad \sigma^3 = \begin{pmatrix} 1 & 0 \\ 0 & -1 \end{pmatrix}. \tag{1.4}$$

I use the standard 'slash' notation to contract four vectors with γ^μ:

$$\not{p} \equiv p_\mu \gamma^\mu. \tag{1.5}$$

The momentum operator I use the notation

$$p^\mu = i\partial^\mu, \tag{1.6}$$

where

$$\partial^\mu = \left(\frac{\partial}{\partial x^0}, -\nabla \right) = \left(\frac{\partial}{\partial x^0}, \frac{\partial}{\partial x^1}, \frac{\partial}{\partial x^2}, \frac{\partial}{\partial x^3} \right). \tag{1.7}$$

<center>**Chapter 2**</center>

<center>**Strongly Coupled Physics Beyond the Standard Model**</center>

2.1   The Standard Model

In our current understanding of the universe there are four fundamental forces in nature: gravity, electromagnetism, the strong nuclear force, and the weak nuclear force. The latter three forces are understood in terms of quantum field theories which form the Standard Model (SM). The Standard Model is a $SU(3)_c \times SU(2)_W \times U(1)_Y$ gauge theory.

The $SU(3)_c$ component of the theory explains the strong nuclear force, also called quantum chromodynamics (QCD). QCD is a $SU(3)$ Yang Mills theory with fermions in the fundamental representation. This force explains how spin 1/2 quarks possessing 'color' charge interact by exchanging gluons. It is important to note that this color charge has nothing to do with visible colors and is analogous to electric charge. Unlike electric charge which can be expressed by only one number, color charge is expressed by three numbers commonly labeled R, G, B, for red, green, and blue respectively. The Lagrangian for QCD is

$$\mathcal{L} = \frac{1}{4g^2} F^a_{\mu\nu} F^{\mu\nu,a} + \sigma_j \bar{\psi}_j (i\gamma^\mu D_\mu + m_j) q_j, \tag{2.1}$$

where

$$G^a_{\mu\nu} = \tag{2.2}$$

, and

$$D_u = \tag{2.3}$$
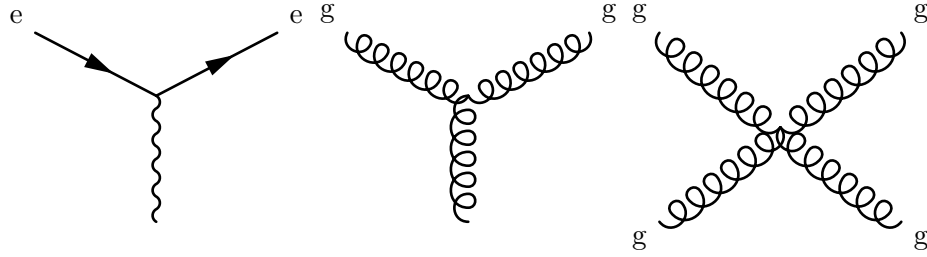
Figure 2.1: here

. A^μ are the gluon fields, ψ_j is the jth quark flavor. μ and ν are the usual spacetime indices while a,b and c are color indices.

The Lagrangian allows the three vertices shown in figure 2.1. The first vertex couples a fermion to a gluon and is analogous to diagrams in QED that couple an electron to the photon. The other two vertices have no analogue in QED, these are the three and four gluon vertices. The gluon vertices consequence of the gluons having a charge anti-charge moment. A repercussion of the gluons being charged is that the color field is anti-screened.

QCD exhibits two interesting properties: confinement and asymptotic freedom. Confinement means that the force between two quarks does not diminish as they are pulled apart. In fact if you try to pull two quarks apart eventually there will be enough energy in the field to produce a new quark anti quark pair. As a result we never observe free quarks in nature, they only exist in colorless bound states called hadrons. Hadrons come in two varieties $q\bar{q}$ pairs called mesons and qqq triplets called baryons. Despite the fact that confinement is easy to demonstrate on the lattice, there is an outstanding Millennium Prize for an analytic proof. Asymptotic freedom reflects that at very large momentum transfers the quarks and gluons interract weakly. This is described by the β function and is elaborated on in section **??**.

The strong nuclear force is responsible for the proton, composed of two up and one down quark, and neutron, composed of two down and one up quark. Additionally, the strong nuclear force binds these particles together to form atomic nuclei. Most of the understood mass in the universe is a result of the strong nuclear force. In QCD the up and down quarks have masses on the order of an MeV while the proton has a mass of 938GeV. Almost all of the proton mass results
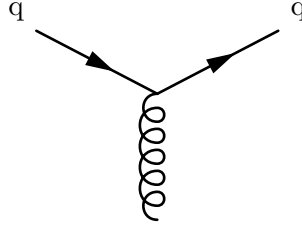
Figure 2.2: here

from its own binding energy.

The remaining $SU(2)_W \times U(1)_Y$ part of the standard model is the electroweak force. This is the quantum field theory that explains the quantum theory of electrodynamics and how particles decay via the weak process. An essential feature of the electroweak theory is that $SU(2)_W \times U(1)_Y$ spontaneously breaks down to $U(1)_{EM}$ see section 2.2 for further details. This breaking gives the $W^{\pm}$ and Z bosons their mass and also accounts for SM fermion masses. $U(1)_E M$ is the theory of quantum electrodynamics in which spin 1/2 fermionic matter charged with electric charge interact by exchanging photos. Unlike in QCD photons are not charged under U(1) and therefore don't interact at tree level. This yields a much simpler theory than QCD and can be understood perturbatively.

The Lagrangian for QED is similar to 2.1 however the field strength tensor $F^a_{\mu\nu}$ is replaced by $F_{\mu\nu}$, dropping the color indices. The simpler Abelian U(1) symmetry also means that the field strength tensor is defined as

$$F_{\mu\nu} = \partial_\mu A_\nu - \partial_\nu A_\mu \tag{2.4}$$

Where A^μ is the four potential defined as $A^\mu \equiv (\phi, \vec{A})$. Only one vertex is allowed that couples a fermion to a photon.

In both the QCD and Electroweak sector matter is divided into three generations of matter. The first generation of matter is the most familiar. It consists of the up quark down quark, electron, and electron neutrino. All of the matter that we experience in our daily lives is made of this generation of matter. The other two generations of matter are essentially heavier replicas of the first generation. These heavier generations rapidly decay via the weak nuclear force to the first

generation of matter and therefore are only detected in high energy events such as cosmic rays or particle physics experiments. The second generation consists of the strange quark, charm quark, muon, and muon neutrino. Finally the third consists of the top quark, bottom quark, tau, and tau neutrino. The properties of all the standard model particles is summarized in table **??**.

INSERT TABLE OF SM PARTICLES

2.2   Higgs Mechanism

In the standard model the $W^{\pm}$ and Z bosons are massive but the photon is massless. Since gauge invariance dictates that a mass term is forbidden in the Lagrangian this seems to pose a problem. Disaster is averted because $SU(2)_W x U(1)_Y$ is spontaneously broken to $U(1)_{EM}$. In the standard model this is accomplished by adding a complex scalar doublet field to the theory. The field is named the Higgs field after one of its discoverers. The following discussion shows how electroweak symmetry breaking is facilitated by the Higgs [**?, ?, ?**].

Lets introduce a complex elementary scalar doublet $\Phi = \begin{pmatrix} \phi^+ \\ \phi_0 \end{pmatrix}$ that transforms in the $(1,2,\frac{1}{2})$ representation of $SU(3)_c \times SU(2)_L \times U(1)_Y$. We allow all terms in the Lagrangian that have mass dimension ≤ 4, thus ignoring irrelevant operators,

$$\mathcal{L}_H = (D_\mu \Phi)^\dagger (D^\mu \Phi) + \mu^2 \Phi^\dagger \Phi - |\lambda|(\Phi^\dagger \Phi)^2, \tag{2.5}$$

with covariant derivative

$$D_\mu \Phi = (\partial_\mu - ig A^a_\mu \tau^a - \frac{ig'}{2} B_\mu)\Phi. \tag{2.6}$$

A^a_μ and B_μ are the $SU(2)$ and $U(1)$ gauge bosons respectively. The coupling constant g belongs to $SU(2)$ and the coupling constant g' belongs to $U(1)$. Finally τ^a are the generators of $SU(2)$ and are related to the Pauli matrices

$$\tau^a = \frac{1}{2}\sigma^a. \tag{2.7}$$

We can now identify the potential $V(\Phi)$ as

$$V(\Phi) = -\mu^2 \Phi^\dagger \Phi + |\lambda|(\Phi^\dagger \Phi)^2, \tag{2.8}$$

this potential is shown in figure **??**. As long as μ^2 is positive the potential has a spontaneously broken symmetry. Gauge invariance allows us to choose the vacuum state to correspond to the vacuum expectation value

$$\langle \Phi \rangle_0 = \frac{\nu}{\sqrt{2}} \begin{pmatrix} 0 \\ \nu \end{pmatrix}, \tag{2.9}$$

where $\nu = \sqrt{\frac{\mu^2}{|\lambda|}}$. Moreover, ν is related to the Fermi constant, G_F, by

$$\nu = \frac{1}{\sqrt{\sqrt{2}G_F}} \approx 246 \text{ GeV}. \tag{2.10}$$

The Higgs Boson, a particle excitations of the Higgs field, was recently discovered at the Large Hadron Collider (LHC). The Higgs Boson was recently discovered at the Large Hadron Collider. Current experimental results pin the Higgs mass at

2.3 Beyond Standard Model Physics

While the Standard Model is the pinnacle of our current understanding of the universe it is not the last word. There are many phenomena that the standard model does not explain. Furthermore there are theoretically troubling aspects to the standard model that leaves more to be desired.

Perhaps the biggest omission in the standard model is a quantum field theory of Gravity. Our current understanding of gravity is Einstein's theory of General Relativity which is another thoroughly verified theory. General Relativity is incompatible with quantum mechanics, and to date a force carrying boson, the graviton, has eluded detection. A related problem is that gravity is so much weaker than the other three fundamental forces. Another unexplained phenomena is neutrino oscillations. In nature we have observed the flavor of neutrinos to change. These oscillations prove that the neutrino's are not massless particles as the standard model previously had us believe. Finally we currently understand from astrophysical observations that the standard model only accounts for 4% of the energy budget of the universe. Dark matter, which has eluded detection composes of another 20% of the energy budget. Dark Energy, which is responsible for the acceleration of the expansion of the universe composes 75% of our energy budget.

In addition to not explaining the entire range of physical phenomena that we observe (or fail to observe) there are theoretical shortcomings that indicate a lack of complete understanding. The first indication that something is awry is the number of parameters. The standard model in its most general form has ninteen free parameters. All of these parameters are fixed by experiment and cover a large range. We expect that a more nuanced understanding of the unverise will require less parameters.

Another theoretical quirk of the standard model is the strong CP problem. Unlike the electroweak interractions, QCD does not violate CP symmetry. CP symmetry is the symmetry of charge conjugation (C) and parity (P). The QCD Lagrangian allows terms that violate CP symmetry but these terms appear to be zero which is a type of fine tuning.

Finally there is the heirarchy problem. In the standard model the coupling constants of the theory change with energy scale. If you run the theory into the UV the coupling constatns nearly converge at the GUT scale of 10^{16} GeV. The standard model can be run further to the plank scale and it remains a conssitent theory. The fact remains that the standard model is an effective theory and at some point it must be cut off. The cutoff of the theory is removed from several orders of magnitude from the weak scale. This is a problem because the Higgs is an elementary scalar field and therefore has a relevant quartic self coupling. As a result the Higgs has a quadratically divergent additive renormalization to its mass. To keep the renormalized Higgs mass at its physical value an unnatural degree of fine tuning to its bare mass is required.

These issues have pushed researchers to look for extensions or alternatives to the standard model that answer one or more of these unresolved questions. One area of active research has been the hierarchy problem. The state of affairs for almost 40 years was that we knew there had to be a Higgs mechanism to complete the standard model. We also had a very good guess where to look for the Higgs boson because of the mass of the $W^{\pm}$ and the Z. Solving the heirarchy problem and predicting the Higgs mass became a popular game, guess right and win a Nobel Prize. Most methods of solving the heirarchy probelm introduce new physics at the electroweak scale. This moves the SM cutoff much closter to the electroweak scale, removing the issue of fine tuning. Super

Symmetry is one such approach that postulates a symmetry between fermions and bosons. This symmetry results in a cancelation of the quadratic divergence that the scalar Higgs theory has. Another approach which I will describe further in the next section is for the Higgs particle to be a composite particle. A consequence of all of these theories is new particles. Now we know the value of the Higgs mass and no other particles have been discovered by the LHC yet, ruling out the simplest incarnations of these models.

2.4   Composite Higgs

One solution to the heirarchy problem is for the Higgs to be a composite composed of particles from a new strongly interacting sector. This new sector is responsible for electroweak symmetry breaking. There are many types of theories that use such a modus operandi. While these theories have the benefits of ... they typically favor a heavier Higgs mass than what has been observed. Additionally, these theories are highly constrained by precision electroweak measurements. In the next three subsections I will give a flavor for two classes of composite Higgs theories, introduce the conformal window, and discuss the state of Lattice endeavors in this area.

2.4.1   Technicolor and Extended Technicolor

2.4.2   Conformal Window

A general class of strongly interracting theories that are of interest for technicolor and extended technicolor dynamics are Yang-Mills gauge theories. Pure gauge Yang-Mills theories have $SU(N_c)$ interractions while more general theories include N_f flavors of fermions in some representation. At low energies QCD is effectively a $SU(3)$ gauge theory with N_f=2. This description includes only the up and down quarks which are nearly massless and respect an approximate $SU(2)$ isospin symmetry. The most general Yang-Mills Lagrangian with a $SU(N_c)$ local gauge symmetry and N_f flavors of massless fermions in a representation R is:

$$\mathcal{L}_{YM} = -\frac{1}{4g^2} \sum_{a=1}^{N_c} F_{\mu\nu}^a F^{\mu\nu,a} + \sum_{i=1}^{N_f} \bar{\Psi}_i \left(i \not{D} \right) \Psi_i. \tag{2.11}$$

Representation	dim(R)	$T(R)$	$C_2(R)$
F	N	$\frac{1}{2}$	$\frac{N^2-1}{2N}$
S_2	$\frac{N(N+1)}{2}$	$\frac{N+2}{2}$	$\frac{(N+2)(N-1)}{N}$
A_2	$\frac{N(N-1)}{2}$	$\frac{N-2}{2}$	$\frac{(N-2)(N+1)}{N}$
G	N^2-1	N	N

Table 2.1: this is the caption

The theories allowed by this Lagrangian are similar in the UV but can be dramatically different in the IR. While the Lagrangain is classically scale invariant; the quantum theory is not. This is understood through the beta function,

$$\beta(g^2) = -\mu \frac{\partial g2}{\partial \mu}. \tag{2.12}$$

The beta function describes how the gauge coupling evolves as the renormalization scale μ is changed. This function can be expanded in perturbation theory and is universal to two loops:

$$\beta\left(g^2\right) = -\frac{b_1}{16\pi^2} g^4 - \frac{b_2}{(16\pi^2)^2} g^6 \tag{2.13}$$

Any terms beyond two loops are renormalization scheme dependant and are not relevant for the following discussion. The values for b_1 and b_2 are:

$$b_1 = \frac{11}{3} N_c - \frac{4}{3} N_f T(R) \tag{2.14}$$

$$b_2 = \frac{34}{3} N_c^2 - \frac{4}{3} T(R) N_f \left[5N_c + 3C_2(R) \right]. \tag{2.15}$$

$T(R)$ and $C_2(R)$ are the first and second Casimir invariants and depend on the represenation R of the group. Table 2.4.2 give these invarients for a few common representations.

Clearly tuning N_c, N_f and R offers a great deal of freedom in specifying the gauge theory.

We can see from equation ?? that if the coefficients b_1 and b_2 are both positive than the beta function is negative. In this scenario the theory asymptotically free, confining, and spontaneously

Figure 2.3:

breaks chiral symmetry. The dynamics in the IR will be strongly coupled and nonperturbative. Figure 2.3 shows what this scenario looks like. This occurs in QCD ($SU(3)$ $N_f = 2$ or 3) is an example of a theory where the beta function is negative.

If we keep b_1 positive and allow b_2 to become negative we can force the two terms to compete. Such a beta function would start out negative, then at some coupling it would pass through a local minimum after which it would grow. Eventually the beta function would have a zero where $\beta = 0$. Perturbatively this zero occurs at $g_*^2 = -b_1/b2$ and is a Banks-Zaks infrared fixed point. This is illustrated in 2.4, such a theory is governed by the conformal dynamcis at the infrared fixed point and is scale invarient. Unlike confining theories, such theories do not support bound states of particles.

Allowing both b_1 and b_2 to be negative results in a trivial theory. Such a theory, shown in 2.5 is not asymptotically free. Such a beta function is very similar to that of QED. Perturbatively this occurs when $N_f >$.

The region in theory space between where the IRFP appears and where asymptotic freedom is lost is reffered to as the conformal window. Limmiting our consideration to theories using the

Figure 2.4:

fundamental representaiton fermions and $N_c = 3$ we see that the conformal window is between $N_f = $ and $N_f =$. It is important to note that because of the nature of these theories perturbation theory is not reliable and these numbers only serve as motivation for where to look.

The conformal window itself is not a very interesting system to study but understanding the lower bound of the conformal window is of great interet for potential technicolor theories. Right below the conformal window it is believed that a walking theory can exist. In such a theory, shown in figure 2.6 the beta function would start out like the conformal scenario. However, as the theory approaches the IRFP chiral symmetry is spontateously broken and the beta function would turn around away from the IRFP. This scenario allows

2.4.3 Lattice Studies

There has been a growing interest in studying beyond the standard model theories on the lattices over the past decade. To date there are a number of active lattice groups carrying out caluclations in this field. It is healthy that such a variety of theories have been studied usinging different methods. Beyond standard model physics is inherently a difficult subject to study because
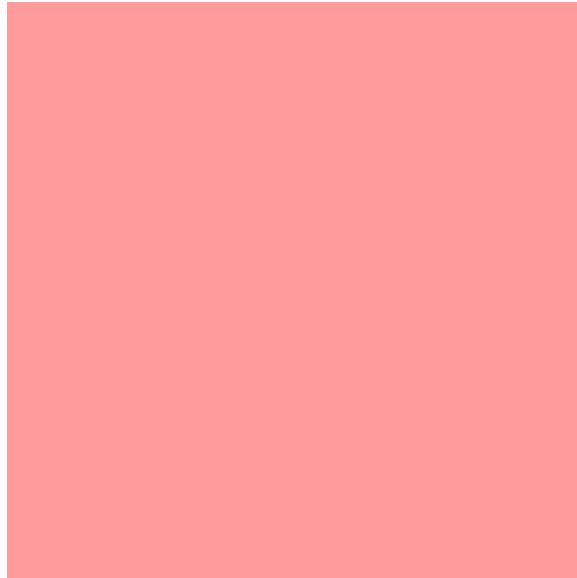
Figure 2.5:

we don't know the answer before hand. Taking a holisitic approach and finding consensus is vital to our understanding. Additionally, as more of these theories have been studied, vital improvements have been made. This is true of the lattice code base which prior to BSM studies was highly optimized and sometimes only available for QCD simulations. Improvements hav also been made in the way the data is analyzed. I will discuss two improvements we have developed in chapters ??-??

As I mentioned above there are a number of ways to appraoch BSM lattice studies. One class of method which I have been involved with is to calculate the beta function directly. There are several ways to calculate the beta function on the lattice. One technique is called the Schrödinger functional. The Schrödinger functional has been widly used to study several theories. Another method is

Another class of methods involve lattice spectroscopy.

Figure 2.6:

Chapter 3

Lattice Field Theory

3.1   The Lattice

Lattice gauge theory is a method to regularize a quantum gauge theory nonperturbatively. To date it is the only controled way to study strongly coupled systems from first principals. Lattice methods have been extremely sucessful in studying the strong nuclear force and many Lattice QCD results are now at the sub percentage accuracy. The lattice regularizes the theory by discretizing Euclidian spacetime onto a regular grid of sites which are connected by links. The most common discritization is that of a four dimensional hypercube. For simplicity I will assume that all the sides of our hypercube are of length L (volume L^4), although this is not necessrary and is infact not true of many lattice calculations.

(anything else to say about discritization?)

path integral formulation

wick rotation

partition function

calculating observables

continuum limit

3.2   Gauge Fields

Gauge action

improvements

3.3   Fermionic Fields

naive fermions

wilson fermions

staggard fermions

nHYP staggered fermions

Chapter 4

Monte Carlo Renormalization Group

4.1   Introduction

In recent years, many groups have initiated lattice investigations of strongly-coupled gauge–fermion systems beyond QCD. While the ultimate goal of these efforts is to explore potential new physics beyond the standard model, an essential step is to improve our theoretical understanding of the basic properties of these non-perturbative systems. In this chapter I study the renormalization group properties of SU(3) gauge theories with $N_f = 8$ and 12 nearly-massless fermions in the fundamental representation, through the Monte Carlo Renormalization Group (MCRG) two-lattice matching technique. This is one of several complementary analyses our group is involved with, two more of which (investigating Dirac eigenmode scaling and finite-temperature transitions) are discussed elsewhere [35, 52]. Recent references on SU(3) gauge theories with $N_f = 8$ and 12 include [23, 24, 4, 21, 42]; earlier works are reviewed in Ref. [30].

References [34, 33] study MCRG two-lattice matching for the 12-flavor system with nHYP-smeared staggered actions very similar to those we use here. Our gauge action includes both fundamental and adjoint plaquette terms, with coefficients related by $\beta_A = -0.25\beta_F$. The negative adjoint plaquette term lets us avoid a well-known spurious ultraviolet fixed point caused by lattice artifacts, and implies $\beta_F = 12/g^2$ at the perturbative level. In our fermion action, we use nHYP smearing with parameters $(0.5, 0.5, 0.4)$, instead of the $(0.75, 0.6, 0.3)$ used by Refs. [34, 33]. By changing the nHYP-smearing parameters in this way, we can access stronger couplings without encountering numerical problems. At such strong couplings, for both $N_f = 8$ and $N_f = 12$ we

observe a lattice phase in which the single-site shift symmetry ("S^4") of the staggered action is spontaneously broken ("$\mathcal{S}^4$") [18, 52].[1] In this work we only investigate couplings weak enough to avoid the $\mathcal{S}^4$ lattice phase.

In the next section, we review how the MCRG two-lattice matching technique determines the step-scaling function s_b in the bare parameter space. Although working entirely with bare parameters would be disadvantageous if our aim were to produce renormalized phenomenological predictions for comparison with experiment, our current explorations of the phase structures of the 8- and 12-flavor systems benefit from this fully non-perturbative RG approach, especially for relatively strong couplings. In Section ?? we present our results from the traditional MCRG two-lattice matching technique. While our 8-flavor s_b is significantly different from zero, for $N_f = 12$ we observe $s_b \lesssim 0$ for $\beta_F < 8$, indicating an infrared fixed point (IRFP).

We emphasize that while the existence of an IRFP is physical (scheme-independent), the coupling at which it is located depends on the choice of renormalization scheme. A limitation of traditional MCRG two-lattice matching is the need to optimize the RG blocking transformation separately for each lattice coupling β_F. As we explain below, this optimization forces us to probe a different renormalization scheme for each β_F, so that the bare step-scaling function we obtain is a composite of many different discrete β functions. Chapter 6 discusses an improvement to traditional MCRG that avoids this issue.

4.2   Method

In this section I will discuss the basic procedure for MCRG. MCRG is a real space renormalization group technique that can be used to study the critical properties of statistical systems. The idea was first proposed by Kadanoff however it wasn't until Wilson's work that it became a well defined quantitative technique. The process of MCRG can be broken into two primary steps:

(1) Blocking

---

[1] Ref. [21] recently interpreted the $\mathcal{S}^4$ lattice phase in terms of relevant next-to-nearest neighbor interactions.

(2) Matching

Blocking integrates out the UV fluctuations, exposing the IR dynamics. Matching allows us to match pairs of couplings in such a way that we can measure the bare step scaling function. The steps scaling function is the discrete analog of the beta function in the continuum. In general it is possible to recover the beta function from the step scaling function. However, for our purposes this is not important. Our goal is to determine whether or not a particular theory is conformal in the IR. As long as strong enough couplings are studied the IRFP will be visible in both the bare step scaling function and the renormalized beta function.

In the Wilsonian picture, couplings are characterized by their engineering dimension. In a four dimensional theory, a coupling is relevant if its engineering dimension is less than four. The coupling is marginal if its engineering dimension is equal to four and irrelevant if the engineering dimension is greater than four. The RG flow of the system is governed by fixed points and the renormalized trajectory. Additionally fixed points can be attractive or repulsive. A repulsive fixed point will push the RG flow along relevant directions. This flow characterizes the renormalized trajectory. Flow in irrelevant directions will always be directed towards the renormalized trajectory. Finally flow along the renormalized trajectory will always flow into attractive fixed points. In theories with multiple fixed points, the renormalized trajectory connects the fixed points in coupling space. Flow from an arbitrary point in coupling space will always be towards the renormalized trajectory in irrelevant or marginal directions and along the renormalized trajectory in relevant directions. Generally the flow should be fastest in irrelevant directions.

4.2.1   Blocking

The first step in MCRG is to block the lattice. Blocking requires that the theory is defined on a regular lattice that has a discrete scaling symmetry. Discrete scaling symmetry, shown in 4.1 simply means that you can divide the sites of the lattice into regular blocks that tile the entire lattice and then replace those blocks with a single site. The new site can be located at a sight from the original lattice or anywhere in the block. The value at this site is typically computed as

some function of the sites in the blocking group. If we perform this replacement the same way to every block in the original lattice and the lattice formed by the block variables is identical after scaling the lattice spacing $a \to a' \equiv sa$ to the original lattice then the system has discrete scaling symmetry. Here s is a scale factor which relates the original lattice to the blocked lattice.
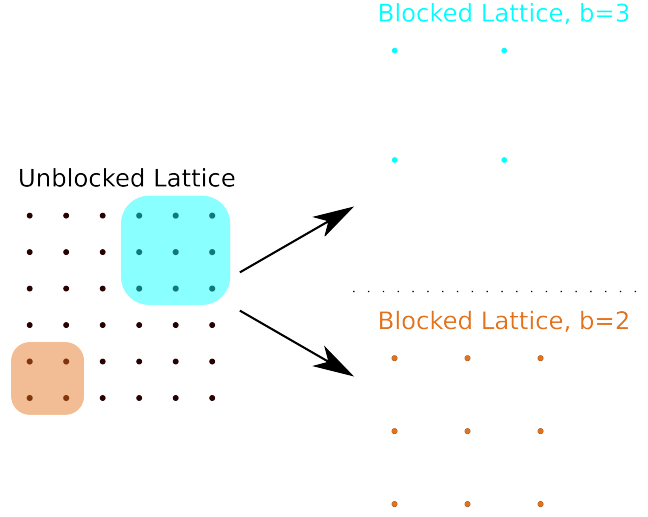
Figure 4.1:

The blocked lattice will have fewer sites than the original lattice. If the block variable has p sites from the original lattice and d dimensions then the relationship between the number of sites lost, the scale factor and the lattice dimension is $p = s^d$. Naturally the blocking process can be repeated in a recursive manner until blocking is no longer possible. As an example consider a 32^2 square lattice that is being blocked by a factor $s = 2$. Such a lattice can be blocked 4 times: $32^2 \to 16^2 \to 8^2 \to 4^2 \to 2^2$. Performing another blocking would result in a single point which doesn't have the same dimensionality as our initial $2-D$ lattice. It is clear that some starting volumes are more flexible than others. An 14^2 lattice can only be blocked once, $14^2 \to 7^2$, 7^2 can not be blocked with a scale factor of 2.

In a lattice simulation the quantities we are interested in are the link variables. The link variable $U_{n,\mu}$ encodes the gauge field at sight n in all four $\hat{\mu}$ directions. A MCRG blocking step is

a transformation that takes two links $U_{n,\mu}$ and $U_{n+\hat{\mu},\mu}$ and creates one link with twice the lattice spacing of the initial two links.
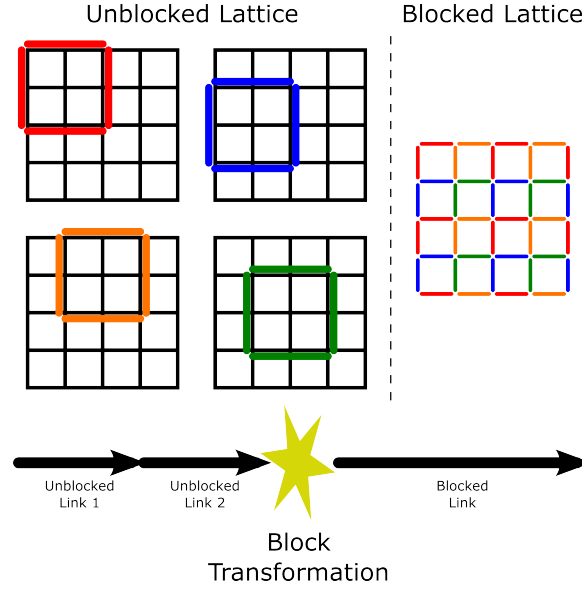
Figure 4.2:

Employing a square blocking scheme as described above means the blocked lattice will have a factor of 2^N less links than the original lattice. In four dimensions this means that an observable such as a Wilson loop will have a factor of 16 less statistics on the blocked lattice compared to the original lattice. Fortunately, on an N dimensional hyper cubic lattice there are 2^N unique ways to perform this blocking. Therefore in four dimensions there are 16 unique blocking configurations. We can preserve statistics in our calculation by performing all of the unique blocking transformations and averaging all of the observables from those blocking transformations together. Additionally we store the blocked links on a lattice of the original cardinality using offsets as shown in 4.4. This allows us to efficiently store a lattice blocked down to any allowable level and has the added benefit that only minor adjustments need to be made to calculate blocked observables.

Lets consider how blocking will effect a lattice model with d dimensions and action $S(K_i)$. Here K_i are the set of all possible couplings in the action. In lattice simulations only a small number of these couplings are actually tuned. The system is characterized by one or more length scales i.e.

the correlation length ξ. After blocking, the links have a lattice spacing scaled by s, $a' = sa$ such that the physical size of the box has not been changed. This removes the UV fluctuations below the length scale sa. Because the UV modes have been integrated out the blocked lattice is described by a new action S' with a new set of couplings $K_i^{n_b}$ where n_b is the number of blocking steps. As long as s is smaller than the lattice correlation length the infrared properties of the system are unaffected. Successive blocking steps will define a flow in coupling space:

$$K_i^{(0)} \to K_i^{(1)} \to K_i^{(2)} \to ... \to K_i^{(n_b)}, \tag{4.1}$$

where K_i^0 denotes the couplings on the unblocked lattice.

Although the physical correlation length is unchanged the lattice correlation length after n_b blocking steps is scaled by

$$\xi^{n_b} = s^{-n}\xi^{(0)}. \tag{4.2}$$

Critical fixed points exist when $\xi = \inf$ and trivial fixed points exist when $\xi = 0$. The scaling behavior at critical fixed points are well understood theoretically. Here the linearized RG transformation predicts the scaling operators and the corresponding scaling dimension.

Figure **??** visualizes the renormalization group flow that I have described for a system with one fixed point and only one relevant coupling at the fixed point, K_0. All other couplings are irrelevant and are collapsed onto the y-axis. The critical surface is shown in the figure is depicted at at $K_0 = 0$. A simulation point in parameter space, p, is chosen. The flow lines approach the fixed point in the irrelevant directions and flow away from the fixed point in the relevant direction. After some number of RG steps the irrelevant operators have died out and the system is flowing along the renormalized trajectory. The renormalized trajectory is uniquely determined by the RG transformation.

Finally, in our blocking step we also apply a nHYP smearing step. By changing the parameters in the smearing step we can control the renormalized trajectory that we will flow to under successive blocking steps. If we start with an infinite volume the choice of nHYP parameters would be of little consequence because we could block our system an infinite number of times until we

reach the renormalized trajectory. Unfortunately in the real world we are not afforded that luxury. It is necessary to choose a smearing that guarantees you reach the renormalized trajectory, more on this in the next section.

4.2.2 Two-lattice matching procedures and the need for optimization

The goal of two lattice matching is to determine a series of lattice couplings, $\beta_0, \beta_1, ... \beta_n, ...$, with lattice spacings that differ by a factor of s between consecutive points. That is $a(\beta_n) = a(\beta_{n-1})/s$. The scale change s is the same scale change from the blocking discussion above. The process is similar to the Schrödinger functional method []. The primary difference is that MCRG is defined through bare couplings while the Schrödinger functional is defined through renormalized couplings. I denote the bare step scaling function as

$$s_b(\beta_n, s) = \beta_n - \beta_{n-1}. \tag{4.3}$$

The renormalized running coupling of theories governed by a Gaussian fixed point can be recovered with a bit of extra work. In weak coupling near the fixed point a renormalized coupling can be calculated. This coupling can be compared to a continuum regularization scheme. At stronger coupling a physical quantity or other quantity such as the Sommer parameter or the Wilson Flow is used to determine the lattice scale. Since the primary focus of this thesis is to determine the existence or lack thereof of an infrared fixed point in strong coupling I don't attempt to follow such a procedure. In the future finding the corresponding renormalized beta function may be of interested.

Figure **??** demonstrates how two lattice matching is performed. In the figure we start with two points in coupling space p_1 and p_2. Under successive RG transformations they flow along the lines indicated. If we can identify two sets of couplings that flow to the same point on the renormalized trajectory after the same number of blocking steps we know that the correlation lengths are identical. From equation 4.2 we know that if two sets of couplings flow to the same point on the renormalized trajectory, but one set of couplings required one less blocking step that

the lattice correlation length differers from a factor of s. Thus we have accomplished our goal. We have identified two points in coupling space p_1 and p_2 with corresponding $\xi_2 = \xi/s$ after n and $(n-1)$ blocking steps.

Demonstrating that the couplings are equal is equivalent to showing that the actions are identical, $S(p_1^{(n_b)}) = S(p_2^{(n_b-1)})$. Calculating the blocked action is extremely challenging. We are saved because we don't need to know the exact form of the actions to demonstrate that they are equivalent. Instead we can show that expectation values of every operator measured on $p_1^{(n_b)}$ and $p_2^{(n_b-1)}$ are identical. Generating configuration ensembles of blocked lattices with Boltzman weights is trivial, we simply need to take an existing ensemble of configurations and then block them [?].

Putting everything together we can prescribe the following procedure for two lattice matching [?]:

(1) Generate a configuration ensemble of size L^d with action $S(p_1)$. Block each configuration n_b times and measure a set of expectation values on the resulting $(L/s^{n_b})^d$ set.

(2) Generate several configurations of size $(L/s)^d$ with action $S(p_2)$, where each p_2 is a trial coupling. Block each configuration (n_b-1) times and measure the same expectation values on the resulting $(L/s^{n_b})^d$ set. Compare the results with that obtained in step 1 and tune the coupling p_2 such that the expectation values agree.

This method is powerful for several reasons. Since we compare measurements on the same lattice size, the finite volume corrections are small. Working on lattices larger than the correlation length of the system is not required. MCRG works in both the confined and deconfined phases. Since the matching is accomplished from measurements of local operators, their computation is cheap and the statistical errors are small. Finally because the flow lines are unique it is sufficient to match only one operator. The other operators should give the same prediction. If we fail to reach the renormalized trajectory it will be evident in that the other operators do not match. Therefore we can use the spread in the matching values of the different operators as a measure a systematic error in our matching.

The discussion so far has focused on fixed points with one relevant operator. If the fixed point has two relevant operators the matching process is identical only now it is necessary to tune two operators to find pairs of points in coupling space. While this is possible it is much easier to fix one of the relevant couplings to its fixed point value. By effectively removing one of the relevant couplings we can proceed as with the matching of the remaining coupling.

There is one final hurdle to overcome. On a finite volume we only have a finite number of blocking steps. If we are unlucky we might choose a block transformation, and therefore a renormalized trajectory, that is so far away from the bare parameters in couplings space. Accordingly after we have performed the maximum number of blocking steps the system may not reach the renormalized trajectory. This is a problem because matching requires both blocked ensembles to have reached the renormalized trajectory.

One solution is to use a bigger volume. Using a bigger volume means that we can perform more blocking steps, eventually we will arrive at the renormalized trajectory. This solution is clearly flawed. Lets assume that the largest volume you have is 32^4 and you can not reach the renormalized trajectory in four blocking steps. To achieve one more blocking step you need to jump to 64^4 lattices, if that is not enough then on to 128^4 lattices. We are now considering lattices that are larger than those used for large professional calculations! The computational cost of configuration generation scales roughly as $V^{5/4}$, in our doubling scenario generating larger volumes will require at least $2^{5/4}$ more computational power.

Clearly we need another solution. As I mentioned above we apply an nHYP smearing step during our block transformation. This serves a crucial role, nHYP smearing has 3 parameters. Since the different block transformations correspond to different renormalized trajectories, tuning the nHYP parameters allows us to control the renormalized trajectory that we flow to. We use the first parameter of the nHYP smearing as an optimization parameter and fix the second and third. We identify the optimal blocking accordingly:

(1) Consistent matching between the different opera- tors: along the RT all expectation values

should agree on the matched configuration sets. Any deviation is a measure that the RT has not been reached.

(2) Consecutive blocking steps should give the same matching coupling.

4.2.3   Chirally Broken Theories
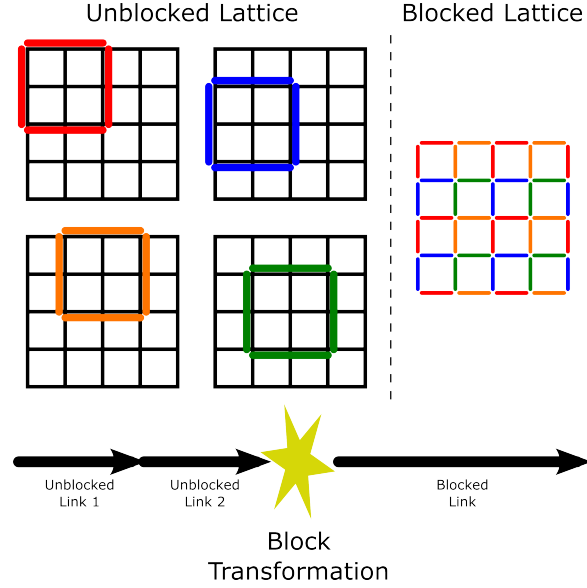
Figure 4.3:

In a confining chiral broken theory, such as QCD, the RG flow will away from the repulsive UV fixed point into the IR. If the fermions are massless the only relevant operator is the gauge coupling β. This is the β that we set in the action of our lattice simulation. Therefore the renormalized trajectory will flow along the β axis in coupling space from infinity to zero. RG flows will flow to the renormalized trajectory and then along it as shown in **??**

4.2.4   Confining Theories

In a conformal system with massless fermions, the RG flow from points on the weak coupling side of the IRFP will also flow towards the renormalized trajectory in irrelevant directions. However unlike the QCD case the flow along the renormalized trajectory will terminate at the IRFP. At the

Unblocked Lattice   Blocked Lattice

Unblocked
Link 1

Unblocked
Link 2

Blocked
Link

Block
Transformation
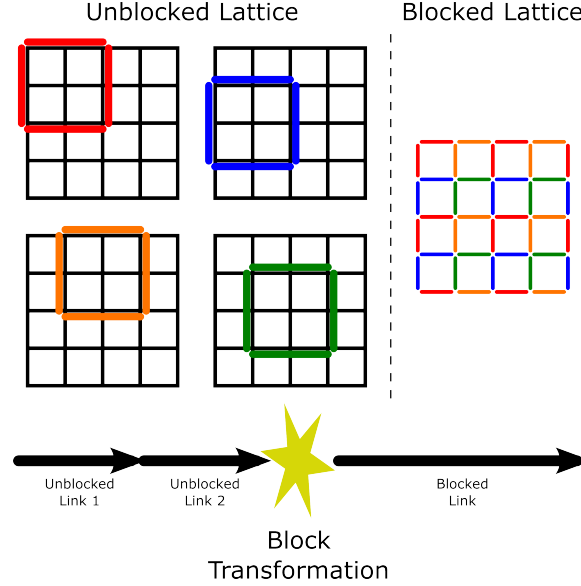
Figure 4.4:

IRFP β also becomes an irrelevant operator. Had we started from the strong coupling side of the IRFP we would observe something completely new. The flow would move towards the renormalized trajectory in the irrelevant directions but it would flow into the IRFP. The flow into the IRFP from the strong coupling is 'backwards' from the flow in a chiral broken theory. The behavior of a conformal theory is shown in figure **??**.

4.3   8 and 12 Flavor Results

In this section I employ the two lattice matching technique described earlier in this chapter to study SU(3) gauge theories with 8 and 12 chiral fermions in the fundamental representation. We proceed by repeatedly applying an nHYP RG blocking transformations with scale factor $s = 2$. The lattices used in this study have volumes $24^3 \times 48$, $12^3 \times 24$ and $6^3 \times 12$. On the largest $24^3 \times 48$ lattices that we use in this current study, we work with fermion masses $m = 0.0025$ to stay near the $m = 0$ critical surface. Under RG blocking with scale factor s, the fermion mass changes as $s^{1+\gamma_m}$ where γ_m is the mass anomalous dimension. Therefore we use $m = 0.01$ on $12^3 \times 24$ and $m = 0.02$ on $6^3 \times 12$ lattices. We have explicitly checked that these masses are small enough to introduce

only negligible finite-mass effects, by generating lattices with $m = 0$ for some points and obtaining indistinguishable results.

Under RG blocking on the $m = 0$ critical surface, the system flows toward the renormalized trajectory in irrelevant directions, and along it in the relevant direction. By blocking the larger lattices (with β_F) n_b times and the smaller lattices (with β'_F) only $n_b - 1$ times, we obtain blocked systems with the same lattice volume. If these blocked systems have both flowed to the same point on the renormalized trajectory, then we can conclude that $\xi(\beta_F) = 2\xi(\beta'_F)$ on the unblocked systems, as desired.

We determine whether the blocked systems have flowed to the same point on the renormalized trajectory by matching several short-range gauge observables: the plaquette, all three six-link loops, and two planar eight-link loops. For a given β_F, each observable may predict a different $\Delta\beta_F \equiv \beta_F - \beta'_F$. The spread in these results is a systematic error that dominates our uncertainties. In principal more observables can be added, our choices are limited by the final volume of the blocked lattice.

In an IR-conformal system, the gauge coupling that is relevant at the perturbative gaussian FP becomes irrelevant at the IRFP. The renormalized trajectory connects these two fixed points. When RG flows approach this renormalized trajectory, the two-lattice matching can be performed and interpreted the same way as in confining systems. In this region the gauge coupling flows to stronger couplings, $\Delta\beta_F > 0$ corresponding to a negative RG β function. The situation is less clear at stronger couplings where we might naïvely expect backward flow. If there is no ultraviolet FP in this region to drive the RG flow along a renormalized trajectory, the two-lattice matching might become meaningless. This issue affects every method that attempts to determine the flow of the gauge coupling in IR-conformal systems at strong coupling. In all published studies that report an IRFP, backward flow has only been observed in a very limited range of couplings in the immediate vicinity of the IRFP (cf. Ref. [30]).

Since we can block our lattices only a few times, we must optimize the two-lattice matching by requiring that consecutive RG blocking steps yield the same $\Delta\beta_F$. We identify the optimized

$\Delta\beta_F$ with the bare step-scaling function s_b. The traditional technique reported in this chapter optimizes the RG blocking transformation (renormalization scheme). The new method we propose in Section 6 instead applies the Wilson flow to the lattice system prior to RG blocking, and optimizes the flow time t_f.

As in Refs. [34, 33], we use RG blocking transformations that include two sequential HYP smearings with parameters $(\alpha, 0.2, 0.2)$, and optimize α as shown in the left panel of Fig. 4.5. Qualitatively, this optimization finds the renormalization scheme for which the renormalized trajectory passes as close as possible to the lattice system with coupling β_F. Without optimization, residual flows in irrelevant directions can distort the results: this is the reason $\Delta\beta_F$ changes with α in Fig. 4.5, and also explains why increasing the number of blocking steps reduces this α-dependence.
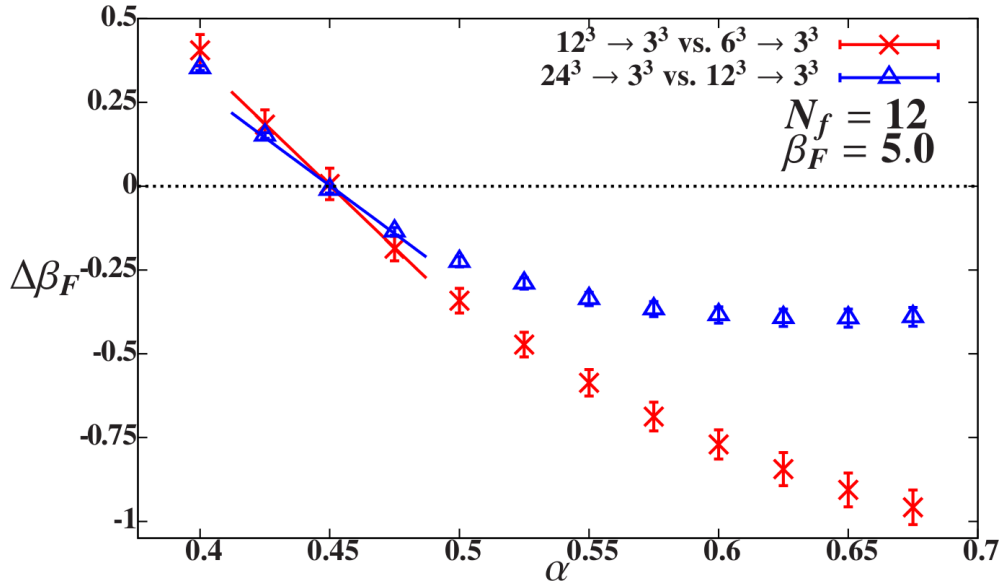
Figure 4.5: Examples of two-lattice matching optimization for 12-flavor systems. Left: Optimization of the HYP-smearing parameter α in the RG blocking transformation, for $\beta_F = 5.0$. Right: Optimization of the Wilson flow time t_f with fixed $\alpha = 0.5$, for $\beta_F = 4.5$. In both cases, the uncertainties on the data points are dominated by averaging over the different observables as described in the text.

We note that finite-volume effects are minimized by carrying out the optimization on blocked lattices of the same volume, which was reported by Ref. [34]. That is, we should compare $\Delta\beta_F$ from matching $12^3 \times 24$ blocked to $3^3 \times 6$ vs. $6^3 \times 12$ blocked to $3^3 \times 6$ with that from matching $24^3 \times 48$

blocked to $3^3 \times 6$ vs. $12^3 \times 24$ blocked to $3^3 \times 6$.

4.3.1 8 Flavors

In our study of SU(3) gauge theories with 8 flavors we calculated the step scaling function at four couplings corresponding to $\beta_F = 5.4, 5.6, 6, 7$. We were unable to perform matching at stronger coupling due to the appearance of the $\mathscr{S}^{\mathscr{A}}$ phase at $\beta_f = 4.6$. At weaker couplings our results for the step scaling function are lower than those predicted by two loop perturbation theory. Perturbation theory predicts a value of $s_b \approx 0.6$. This implies that our simulations are at couplings too strong to perform comparison to perturbation theory. Figure 4.6 displays our final results. The error bars are indicative of the spread the step scaling function predicted by different observables.

It is clear that the step scaling function is far removed from zero. This indicates that the 8 flavor theory does not have an infrared fixed point. While the calculated step scaling function is not in explicit agreement with perturbative value it is somewhat close. Furthermore interpolating between the our measured s_b and the perturbative value does not require a fixed point to develop. This picture is consistent with 8 flavors being chirally broken and confining.

4.3.2 12 Flavors

Our investigation of SU(3) gauge theory with 12 flavors reveals behavior very different from the 8 flavor results.

As in Refs. [34, 33], we do not explore weak enough couplings to recover the two-loop perturbative predictions $s_b \approx 0.3$ for $N_f = 12$.

4.3.3 The Case of the Wandering Fixed Point

The downside of optimizing the RG blocking transformation in this manner is that we have to use a different renormalization scheme for each β_F. As a result, the bare step-scaling function we obtain is a composite of many different discrete β functions. Recall that our optimization of the RG blocking transformation means that we use a different renormalization scheme for each coupling
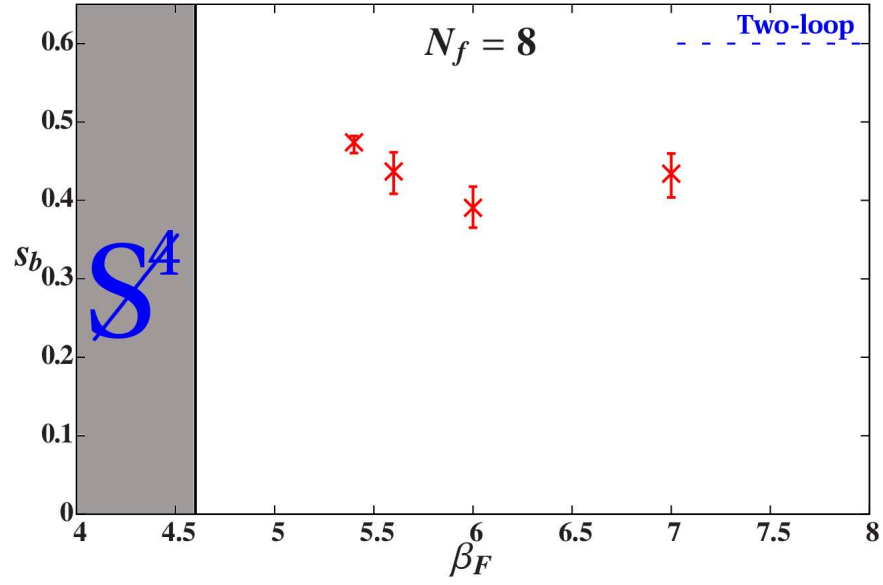
Figure 4.6: Results for the bare step-scaling function s_b from traditional MCRG two-lattice matching with $24^3 \times 48$, $12^3 \times 24$ and $6^3 \times 12$ lattice volumes, for $N_f = 8$ (left) and $N_f = 12$ (right). The blue dashed lines are perturbative predictions for asymptotically weak coupling.
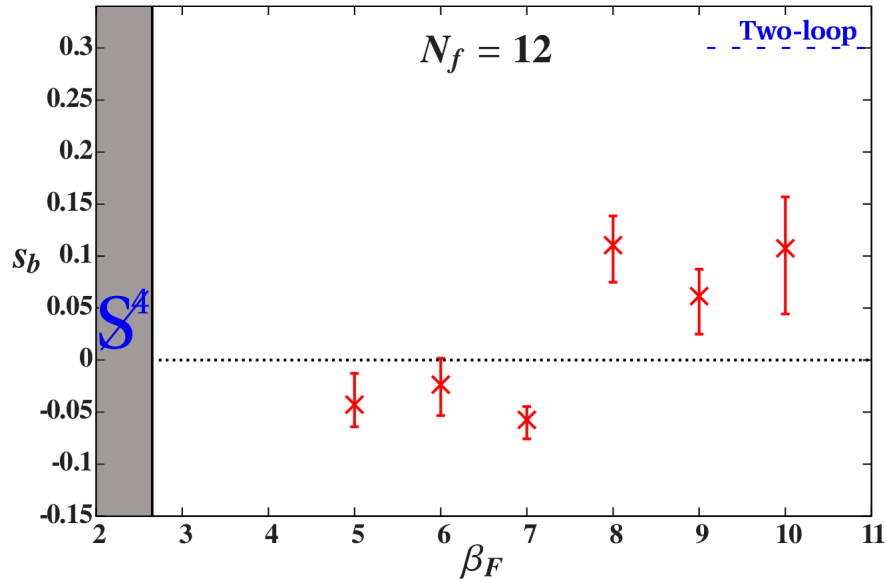
Figure 4.7: Results for the bare step-scaling function s_b from traditional MCRG two-lattice matching with $24^3 \times 48$, $12^3 \times 24$ and $6^3 \times 12$ lattice volumes, for $N_f = 8$ (left) and $N_f = 12$ (right). The blue dashed lines are perturbative predictions for asymptotically weak coupling.

β_F, so these bare step scaling functions are composites of several different discrete β functions. For example, with $N_f = 12$ at $5 \leq \beta_F \leq 6$, our optimization selects renormalization schemes with the fixed point near β_F, so that s_b is roughly consistent with zero over an extended range.

Chapter 5

Wilson Flow

5.1   Introduction

Asymptotically-free SU(N) gauge theories coupled to N_f massless fundamental fermions are conformal in the infrared if N_f is sufficiently large, $N_f \geq N_f^{(c)}$. Their renormalization group (RG) β functions possess a non-trivial infrared fixed point (IRFP) where the gauge coupling is an irrelevant operator. Although this IRFP can be studied perturbatively for large N_f near the value at which asymptotic freedom is lost [13, 11], as N_f decreases the fixed point becomes strongly coupled. Systems around $N_f \approx N_f^{(c)}$ are particularly interesting strongly-coupled quantum field theories, with non-perturbative conformal or near-conformal dynamics. Their most exciting phenomenological application is the possibility of a light composite Higgs boson from dynamical electroweak symmetry breaking [25, 45, 6, 28, 1]. Due to the strongly-coupled nature of these systems, lattice gauge theory calculations are a crucial non-perturbative tool with which to investigate them from first principles. Many lattice studies of potentially IR-conformal theories have been carried out in recent years (cf. the recent reviews [47, 31] and references therein). While direct analysis of the RG β function may appear an obvious way to determine whether or not a given system flows to a conformal fixed point in the infrared, in practice this is a difficult question to address with lattice techniques. In particular, extrapolation to the infinite-volume continuum limit is an essential part of such calculations.

In the case of SU(3) gauge theory with $N_f = 12$ fundamental fermions, several lattice groups have investigated the step scaling function, the discretized form of the β function. To date, these

studies either did not reach a definite conclusion [32, 42] or may be criticized for not properly taking the infinite-volume continuum limit [7, 8, 32, 34, 40, 50]. At the same time, complementary numerical investigations have been carried out, considering for example the spectrum, or bulk and finite-temperature phase transitions [20, 22, 5, 19, 18, 16, 23, 24, 4, 3, 41]. The different groups performing these studies have not yet reached consensus regarding the infrared behavior of the 12-flavor system.

Our own $N_f = 12$ results favor the existence of a conformal IRFP, which we observe in Monte Carlo RG studies [34, 50]. Our zero- and finite-temperature studies of the lattice phase diagram show a bulk transition consistent with conformal dynamics [52, 36]. From the Dirac eigenvalue spectrum [16], and from finite-size scaling of mesonic observables [14], we obtain consistent predictions for a relatively small fermion mass anomalous dimension: $\gamma_m^\star = 0.32(3)$ and $0.235(15)$, respectively. While this conclusion, if correct, would render the 12-flavor system unsuitable for composite Higgs phenomenology, we consider $N_f = 12$ to remain an important case to study. Considerable time and effort has already been invested to obtain high-quality lattice data for the 12-flavor system. Until different methods of analyzing and interpreting these data can be reconciled – or the causes of any remaining disagreements can be clarified – it will not be clear which approaches are most reliable and most efficient to use in other contexts.

The recent development of new running coupling schemes based on the gradient flow [44, 43, 26, 27, 29] provides a promising opportunity to make progress. In this work we investigate step scaling using the gradient flow running coupling.[1] We begin by introducing a non-perturbative improvement to this technique, which increases our control over the continuum extrapolation by reducing the leading-order cut-off effects. While this improvement is phenomenological in the sense that we have not derived it systematically through a full improvement program, it is generally applicable to any lattice gauge theory of interest and can remove all $\mathcal{O}(a^2)$ cut-off effects. We illustrate it first for 4-flavor SU(3) gauge theory, a system where the running coupling has previously

---

[1] We are aware of two other ongoing investigations of the $N_f = 12$ gradient flow step scaling function, by the authors of Ref. [26] and Ref. [42].

been studied with both Wilson [54] and staggered [48, 26, 27] fermions. We then turn to $N_f = 12$, where we show that the infinite-volume continuum limit is well defined and predicts an IRFP. In both the 4- and 12-flavor systems, our improvement can remove all observable $\mathcal{O}(a^2)$ effects, despite the dramatically different IR dynamics. We conclude with some comments on other systems where improved gradient flow step scaling may profitably be applied.

5.2 Improving the Gradient Flow Step Scaling

The gradient flow is a continuous invertible smearing transformation that systematically removes short-distance lattice cut-off effects [44, 43]. At flow time $t = a^2 t_{\text{lat}}$ it can be used to define a renormalized coupling at scale $\mu = 1/\sqrt{8t}$

$$g_{\text{GF}}^2(\mu = 1/\sqrt{8t}) = \frac{1}{\mathcal{N}} \left\langle t^2 E(t) \right\rangle, \tag{5.1}$$

where "a" is the lattice spacing, t_{lat} is dimensionless, and the energy density $E(t) = -\frac{1}{2} \text{ReTr} \left[G_{\mu\nu}(t) G^{\mu\nu}(t) \right]$ is calculated at flow time t with an appropriate lattice operator. We evolve the gradient flow with the Wilson plaquette term and use the usual "clover" or "symmetric" definition of $G_{\mu\nu}(t)$. The normalization $\mathcal{N}$ is set such that $g_{\text{GF}}^2(\mu)$ agrees with the continuum $\overline{\text{MS}}$ coupling at tree level.

If the flow time is fixed relative to the lattice size, $\sqrt{8t} = cL$ with c constant, the scale of the corresponding coupling $g_c^2(L)$ is set by the lattice size. Like the well-known Schrödinger functional (SF) coupling, $g_c^2(L)$ can be used to compute a step scaling function [26, 27, 29]. The greater flexibility of the gradient flow running coupling is a significant advantage over the more traditional SF coupling. A single measurement of the gradient flow will provide g_c^2 for a range of c. In our study we obtain g_c^2 for all $0 \leq c \leq 0.5$ separated by $\delta t_{\text{lat}} = 0.01$. Each choice of c corresponds to a different renormalization scheme, which can be explored simultaneously on the same set of configurations [29].

The normalization factor $\mathcal{N}$ in finite volume has been calculated for anti-periodic boundary conditions (BCs) in refs. [26, 27], and for SF BCs in Ref. [29]. In this work we use anti-periodic

BCs, for which

$$\frac{1}{\mathcal{N}} = \frac{128\pi^2}{3(N^2-1)(1+\delta(c))} \qquad \delta(c) = \vartheta^4\left(e^{-1/c^2}\right) - 1 - \frac{c^4\pi^2}{3}, \qquad (5.2)$$

where $\vartheta(x) = \sum_{n=-\infty}^{\infty} x^{n^2}$ is the Jacobi elliptic function. For $0 \leq c \leq 0.3$ the finite-volume correction $\delta(c)$ computed in Ref. [26] is small, $|\delta(c)| \leq 0.03$. As explained in refs. [26, 27], the RG β function of g_{GF}^2 is two-loop universal with SF BCs, but only one-loop universal with anti-periodic BCs.

At non-zero lattice spacing g_{GF}^2 has cut-off corrections. These corrections could be $\mathcal{O}(a)$ for unimproved actions, and even $\mathcal{O}(a)$-improved actions could have large $\mathcal{O}(a^2[\log a]^n)$-type corrections [9, 10]. In existing numerical studies of staggered or $\mathcal{O}(a)$-improved Wilson fermions the leading lattice corrections appear to be $\mathcal{O}(a^2)$ [29, 53],

$$g_{\mathrm{GF}}^2(\mu; a) = g_{\mathrm{GF}}^2(\mu; a=0) + a^2\mathcal{C} + \mathcal{O}(a^4[\log a]^n, a^4). \qquad (5.3)$$

It is possible to remove, or at least greatly reduce, the $\mathcal{O}(a^2)$ corrections in eq. 5.3 by defining

$$\widetilde{g}_{\mathrm{GF}}^2(\mu; a) = \frac{1}{\mathcal{N}}\left\langle t^2 E(t+\tau_0 a^2)\right\rangle, \qquad (5.4)$$

where $\tau_0 \ll t/a^2$ is a small shift in the flow time. In the continuum limit $\tau_0 a^2 \to 0$ and $\widetilde{g}_{\mathrm{GF}}^2(\mu) = g_{\mathrm{GF}}^2(\mu)$.

There are several possible interpretations of the t-shift in eq. 5.4. The gradient flow is an invertible smearing transformation, so one can consider τ_0 as an initial flow that does not change the IR properties of the system but leads to a new action. The gradient flow coupling $\widetilde{g}_{\mathrm{GF}}^2$ in eq. 5.4 is calculated for this new action. Alternatively one can consider the replacement of $\left\langle t^2 E(t)\right\rangle$ with $\left\langle t^2 E(t+\tau_0 a^2)\right\rangle$ as an improved operator for the energy density. In either case the t-shift changes the $\mathcal{O}(a^2)$ term of $g_{\mathrm{GF}}^2(\mu; a)$. If we expand $\widetilde{g}_{\mathrm{GF}}^2(\mu)$ in $\tau_0 a^2$,

$$\widetilde{g}_{\mathrm{GF}}^2(\mu; a) = \frac{1}{\mathcal{N}}\left\langle t^2 E(t)\right\rangle + \frac{a^2\tau_0}{\mathcal{N}}\left\langle t^2 \frac{\partial E(t)}{\partial t}\right\rangle, \qquad (5.5)$$

and choose τ_0 such that the second term in eq. 5.5 cancels the $a^2\mathcal{C}$ term in eq. 5.3, we remove the leading lattice artifacts

$$\widetilde{g}_{\mathrm{opt}}^2(\mu; a) = g_{\mathrm{GF}}^2(\mu; a=0) + \mathcal{O}(a^4[\log a]^n, a^4). \qquad (5.6)$$

Full $\mathcal{O}(a^2)$ improvement through a systematic improvement program would require adding terms to improve the flow equation, the action, the boundary conditions, and the energy density operator $\langle t^2 E(t) \rangle$ [53]. Since our proposed improvement involves only a single parameter τ_0, this τ_0 itself must depend on other parameters, most importantly on $\widetilde{g}_{\mathrm{GF}}^2(\mu)$ and on the bare coupling through the lattice spacing dependence of the term $\left\langle t^2 \frac{\partial E(t)}{\partial t} \right\rangle$ in eq. 5.5. Optimizing τ_0 both in the renormalized and bare couplings could remove the predictive power of the method. Fortunately, as we will see in the next section, our numerical tests indicate that it is sufficient to choose τ_0 to be a constant or only weakly $\widetilde{g}_{\mathrm{GF}}^2(\mu)$ dependent to remove most $\mathcal{O}(a^2)$ lattice artifacts.

Since the gradient flow is evaluated through numerical integration, the replacement $g_{\mathrm{GF}}^2 \to \widetilde{g}_{\mathrm{GF}}^2$ can be done by a simple shift of t without incurring any additional computational cost. The optimal t-shift τ_{opt} can be identified by a simple procedure when the gradient flow is used for scale setting, which we will consider in a future publication. In this paper we concentrate on the step scaling function and find the τ_{opt} that removes the $\mathcal{O}(a^2)$ terms of the discrete β function corresponding to scale change s,

$$\beta_{\mathrm{lat}}(g_c^2; s; a) = \frac{\widetilde{g}_c^2(L; a) - \widetilde{g}_c^2(sL; a)}{\log(s^2)}. \tag{5.7}$$

5.3   4 Flavor Test

We illustrate the t-shift improvement with the $N_f = 4$ SU(3) system. This theory was recently studied by refs. [26, 27] using gradient flow step scaling with staggered fermions. The 4-flavor SF running coupling was previously considered in Ref. [54] using $\mathcal{O}(a)$-improved Wilson fermions, and in Ref. [48] using staggered fermions. In our calculations we use nHYP-smeared [39, 38] staggered fermions and a gauge action that includes an adjoint plaquette term in order to move farther away from a well-known spurious fixed point in the adjoint–fundamental plaquette plane [18]. As in Ref. [26] we impose anti-periodic BCs in all four directions, which allows us to carry out computations with exactly vanishing fermion mass, $m = 0$. For the discrete β function we consider the scale change $s = 3/2$ and compare lattice volumes $12^4 \to 18^4$, $16^4 \to 24^4$ and $20^4 \to 30^4$.
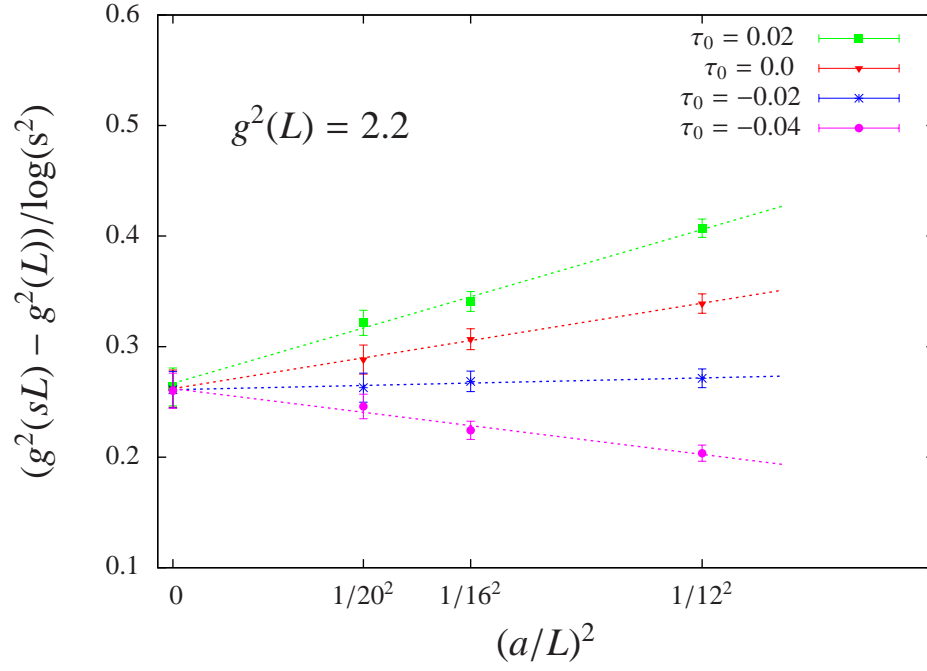
Figure 5.1: Continuum extrapolations of the discrete β_{lat} function of the $N_f = 4$ system at $\widetilde{g}_c^2(L) = 2.2$ with several different values of the t-shift coefficient τ_0. The dotted lines are independent linear fits at each τ_0, which predict a consistent continuum value.
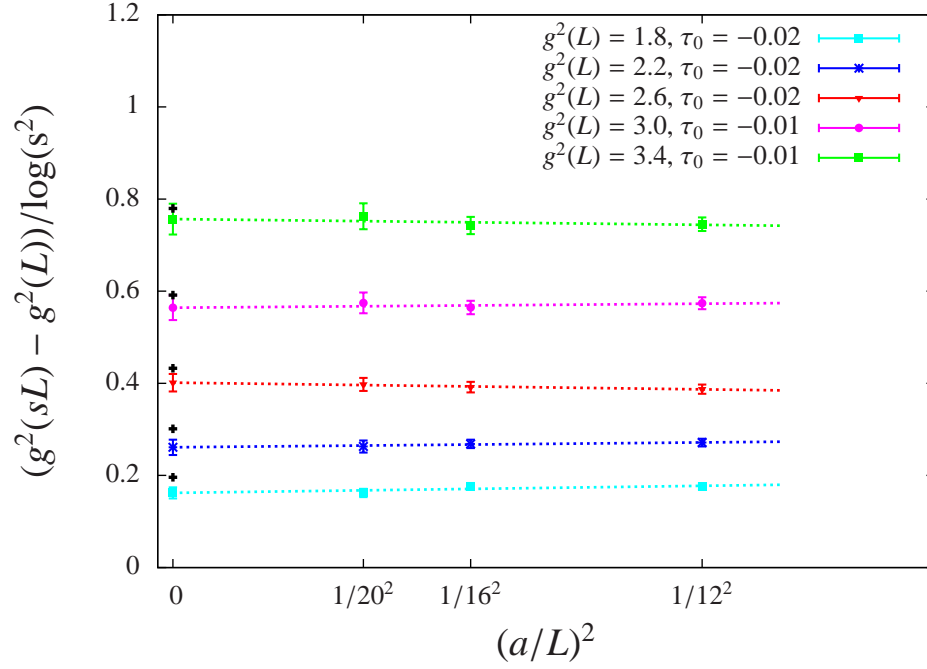
Figure 5.2: Continuum extrapolations of the discrete β_{lat} function of the $N_f = 4$ system for several different $\widetilde{g}_c^2(L)$ values. For $\widetilde{g}_c^2(L) = 1.8$, 2.2 and 2.6 $\tau_0 = -0.02$ is near-optimal, while the larger couplings $\widetilde{g}_c^2(L) = 3.0$ and 3.4 require $\tau_0 = -0.01$ to remove most $\mathcal{O}(a^2)$ effects. The colored points at $(a/L)^2 = 0$ are the continuum extrapolated results, while the black crosses at $(a/L)^2 = 0$ show the corresponding two-loop perturbative predictions.

We accumulated 500–600 measurements of the gradient flow coupling, with each measurement separated by 10 molecular dynamics time units (MDTU), at 7–8 values of the bare gauge coupling on each volume. We consider the $c = 0.25$ scheme, as opposed to $c = 0.3$ used in Ref. [26], because smaller c gives better statistics at the expense of larger lattice artifacts. As discussed above, we aim to reduce these lattice artifacts through the non-perturbative improvement we have introduced. We follow the fitting procedure described in Ref. [54].

Full details of this study will be presented in Ref. [15]. Here we provide a representative illustration of the t-shift optimization. Figure 5.1 shows the dependence of the discrete β function on $(a/L)^2$ when $\widetilde{g}_c^2(L) = 2.2$ with several values of the t-shift parameter τ_0. The red triangles correspond to no improvement, $\tau_0 = 0$. The data are consistent with linear dependence on a^2 and extrapolate to $0.262(17)$, about 2σ below the two-loop perturbative value of 0.301. The slope of the extrapolation is already rather small, $b = 11(3)$. By adding a small shift this slope can be increased or decreased. With $\tau_0 = -0.02$ no $\mathcal{O}(a^2)$ effects can be observed – the corresponding slope is $b = 1.5(3.1)$ – and we identify this value as near the optimal τ_{opt}. The data at different τ_0 extrapolate to the same continuum value, even when the slope b is larger than that for $\tau_0 = 0$. This is consistent with the expectation that the t-shift changes the $\mathcal{O}(a^2)$ behavior of the system but does not affect the continuum limit. Since our action produces relatively small $\mathcal{O}(a^2)$ corrections even without improvement, the t-shift optimization has little effect on the continuum extrapolation, though the consistency between different values of τ_0 is reassuring.

It is interesting that the cut-off effects in our unimproved results, characterized by the slope b of the red triangles in Fig. 5.1, are more than three times smaller than those shown in fig. 4 of Ref. [26]. This difference grows to about a factor of four when we consider the larger $c = 0.3$ used in that study, suggesting that the t-shift optimization could have a more pronounced effect with the action used in Ref. [26]. The cause of the reduced lattice artifacts with our action is not obvious. Both our action and that used by Ref. [26] are based on smeared staggered fermions, though we use different smearing schemes. The different smearing might have an effect, as might the inclusion of the adjoint plaquette term in our gauge action. This question is worth investigating in the future.

In principle τ_{opt} could be different at different g_c^2 couplings but in practice we found little variation. Figure 5.2 shows near-optimal continuum extrapolations of the discrete β function at several values of $\widetilde{g}_c^2(L)$. At each $\widetilde{g}_c^2(L)$ the continuum extrapolated result is consistent within $\sim 2\sigma$ with the two-loop perturbative prediction, denoted by a black cross in Fig. 5.2. Comparable consistency with perturbation theory was found in previous studies [54, 48, 26, 27].

5.4   12 Flavor Results

We use the same lattice action with $N_f = 12$ as with $N_f = 4$ and consider six different volumes: 12^4, 16^4, 18^4, 24^4, 32^4 and 36^4. This range of volumes allows us to carry out step scaling analyses with scale changes $s = 4/3$, $3/2$ and 2. As for $N_f = 4$ we performed simulations in the $m = 0$ chiral limit with anti-periodic BCs in all four directions. Depending on the volume and bare coupling β_F we accumulated 300–1000 measurements of the gradient flow coupling g_c^2 for $0 \le c \le 0.5$, with 10 MDTU separating subsequent measurements. Here we will consider only $c = 0.2$. Full details of our ensembles and measurements, studies of their auto-correlations, and additional analyses for $c = 0.25$ and 0.3 will appear in Ref. [15]. The choice of $c = 0.2$ minimizes the statistical errors, and we find the IRFP in this scheme to be at a weaker coupling than for larger c, which is numerically easier to reach. The typical trade-off for these smaller statistical errors would be larger cut-off effects, but as discussed in previous sections these cut-off effects can be reduced by our non-perturbative improvement.

Figure 5.3 shows the running coupling $g_c^2(L)$ as the function of the bare gauge coupling β_F for different volumes. The interpolating curves are from fits similar to those in Ref. [54]. The curves from different volumes cross in the range $6.0 \le \beta_F \le 6.5$. The crossing from lattices with linear size L and sL defines the finite-volume IRFP coupling $g_\star^2(L; s)$:

$$g_c^2(L) = g_c^2(sL) \implies g_\star^2(L; s) = g_c^2(L). \tag{5.8}$$

If the IRFP exists in the continuum limit then the extrapolation

$$\lim_{(a/L)^2 \to 0} g_\star^2(L; s) \equiv g_\star^2 \tag{5.9}$$
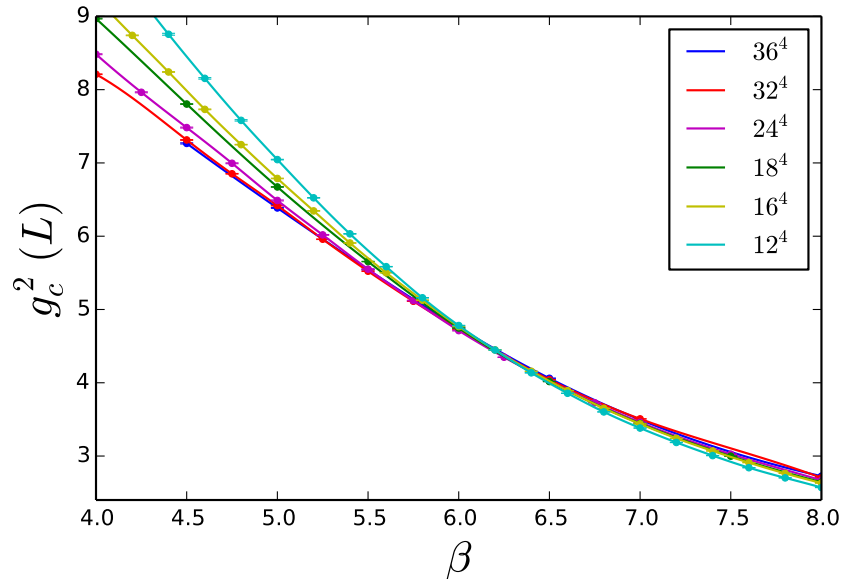
Figure 5.3: The $N_f = 12$ running coupling $g_c^2(L)$ versus the bare coupling β_F on several volumes, for $c = 0.2$. Crossings between results from different volumes predict the finite volume IRFP coupling $g_\star^2(L)$ in this scheme.

has to be finite and independent of s.[2]   Figure 5.4 illustrates the continuum extrapolation of $g_\star^2(L)$ with scale change $s = 2$ for various choices of the t-shift parameter τ_0. The red triangles correspond to no shift, $\tau_0 = 0$. Their $(a/L)^2 \to 0$ continuum extrapolation has a negative slope, and the leading lattice cut-off effects are removed with a positive t-shift, $\tau_{\mathrm{opt}} \approx 0.04$. A joint linear extrapolation of the $\tau_0 = 0$, 0.02, 0.04 and 0.06 results, constrained to have the same continuum limit at $(a/L)^2 = 0$, predicts $g_\star^2 = 6.21(25)$. However, these results all come from the same measurements, and are therefore quite correlated. While it is an important consistency check that the continuum limit does not change with τ_{opt}, just as for $N_f = 4$, the uncertainty in the continuum-extrapolated $g_\star^2$ from this joint fit is not reliable.

Instead, we should consider only the results with the near-optimal $\tau_{\mathrm{opt}} \approx 0.04$. As we show in Fig. 5.5, $\tau_{\mathrm{opt}} \approx 0.04$ is also near-optimal for scale changes $s = 3/2$ and $4/3$. None of these results have any observable $\mathcal{O}(a^2)$ effect, making the extrapolation to the continuum very stable. Each scale change predicts a continuum IRFP for $N_f = 12$. The three sets of results in Fig. 5.5 come from matching different volumes, making a joint fit legitimate. This continuum extrapolation predicts that the IR fixed point is located at renormalized coupling $g_\star^2 = 6.18(20)$ in the $c = 0.2$ scheme.

5.5   Summary

We have considered step scaling based on the gradient flow renormalized coupling, introducing a non-perturbative $\mathcal{O}(a^2)$ improvement that removes, or at least greatly reduces, leading-order cut-off effects. This phenomenological improvement increases our control over the extrapolation to the infinite-volume continuum limit, as we demonstrated first for the case of SU(3) gauge theory with $N_f = 4$ massless staggered fermions. Turning to $N_f = 12$, we found that the continuum limit was well defined and predicted an infrared fixed point even without improvement. Applying our proposed improvement reinforced this conclusion by removing all observable $\mathcal{O}(a^2)$ effects. For the finite-volume gradient flow renormalization scheme defined by $c = 0.2$, we find the continuum

---

[2] We thank D. Nógrádi for useful discussions of the continuum limit.
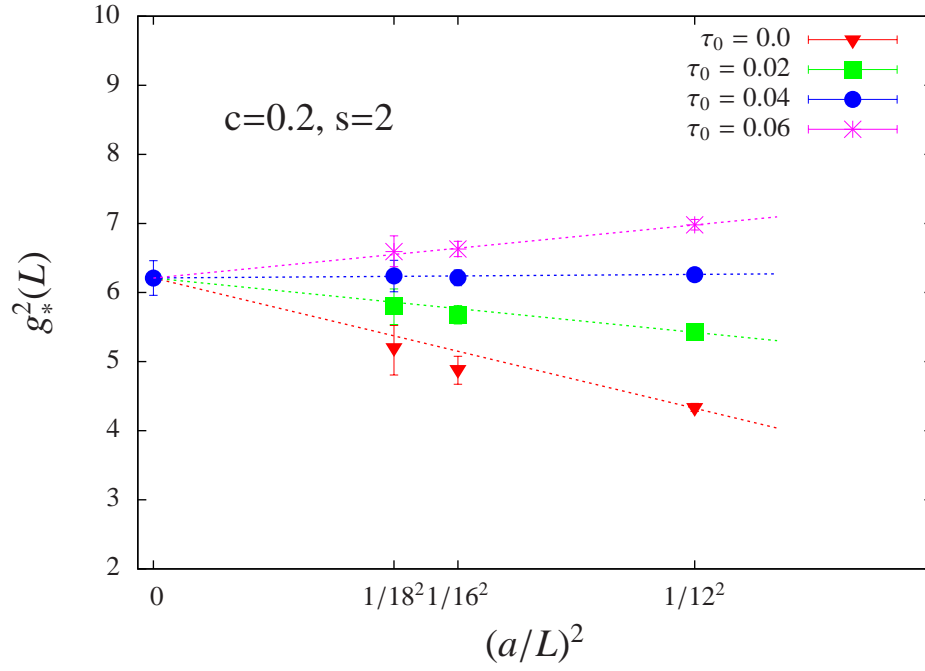
Figure 5.4: Continuum extrapolations of the 12-flavor finite volume IRFP $g_\star^2(L)$, with several different t-shift coefficients τ_0 for fixed scale change $s = 2$. The dotted lines are a joint linear fit constrained to have the same $(a/L)^2 = 0$ intercept, which gives $g_\star^2 = 6.21(25)$.

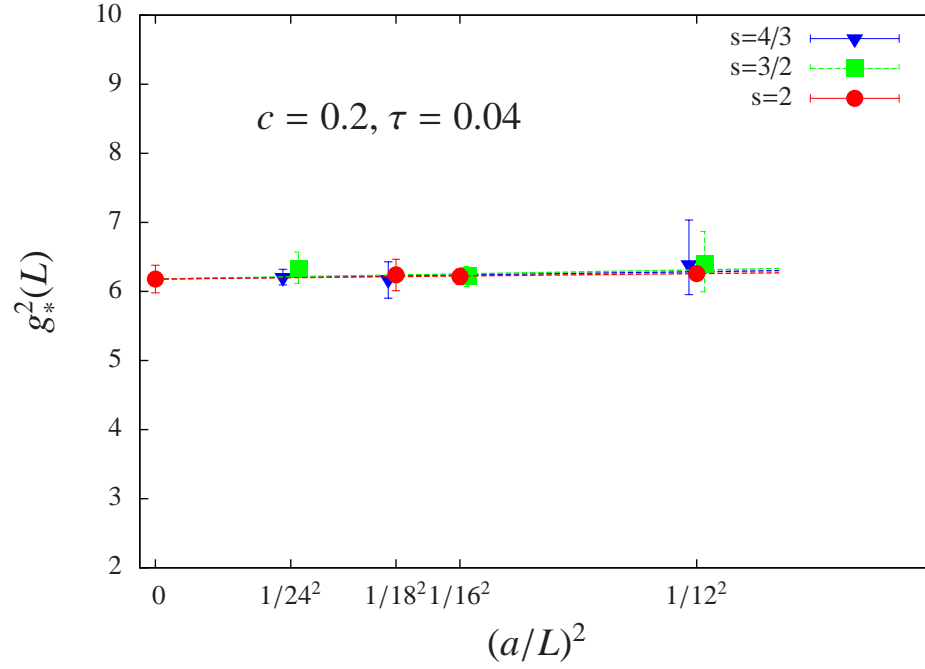Figure 5.5: Continuum extrapolations of the 12-flavor finite volume IRFP $g_*^2(L)$, with several different scale changes for the near-optimal improvement coefficient $\tau_{\mathrm{opt}} \approx 0.04$. The $s = 4/3$ and $3/2$ data points are horizontally displaced for greater clarity. The dashed lines are a joint linear fit constrained to have the same $(a/L)^2 = 0$ intercept, which gives $g_\star^2 = 6.18(20)$.

conformal fixed point to be located at $g_\star^2 = 6.18(20)$.

The 12-flavor system has been under investigation for some time, and other groups have studied its step scaling function [42, 7, 8, 40]. However, this work is the first to observe an IRFP in the infinite-volume continuum limit. There are likely several factors contributing to this progress. While we did not invest more computer time than other groups, we have employed a well-designed lattice action. The adjoint plaquette term in our gauge action moves us farther away from a well-known spurious fixed point, while nHYP smearing allows us to simulate at relatively strong couplings. The gradient flow coupling itself appears to be a significant improvement over other schemes,[3] and our non-perturbative improvement also contributes to obtaining more reliable continuum extrapolations.

Our non-perturbative improvement is general and easy to use in other systems. It does not rely on the lattice action or fermion discretization, though we suspect that the improvement may not be effective if there are $\mathcal{O}(a)$ artifacts, e.g. for unimproved Wilson fermions. Since $\mathcal{O}(a)$-improved lattice actions are standard, this does not appear to be a practical limitation. We look forward to seeing our proposal applied both to QCD and to other conformal or near-conformal systems.

---

[3] C.-J. D. Lin has told us about dramatic improvements in auto-correlations when using the gradient flow coupling compared to the twisted Polyakov loop coupling of Ref. [42].

Chapter 6

Wilson Flow MCRG

6.1   Introduction

For the past several years many lattice groups have been involved in studying strongly-coupled near-conformal gauge–fermion systems. Some of these models may be candidates for new physics beyond the standard model, while others are simply interesting non-perturbative quantum field theories. Because the dynamics of these lattice systems are unfamiliar, it is important to study them with several complementary techniques. Not only does this allow consistency checks, it can also provide information about the most efficient and reliable methods to investigate near-conformal lattice theories.

Monte Carlo Renormalization Group (MCRG) two-lattice matching is one of several analysis tools that we are using to investigate SU(3) gauge theories with many massless fermion flavors. This technique predicts the step-scaling function s_b in the bare parameter space. In a previous work [49] we proposed an improved MCRG method that exploits the Wilson flow to obtain a bare step-scaling function that corresponds to a unique discrete β function. We briefly review our Wilson-flow-optimized MCRG (WMCRG) procedure in Sections ??–??. It is important to note that we are investigating a potential infrared fixed point (IRFP) where the coupling is irrelevant: its running slows and eventually stops. This is challenging to distinguish from a near-conformal system where the gauge coupling runs slowly but does not flow to an IRFP. The observation of a backward flow that survives extrapolation to the infinite-volume limit could provide a clean signal. In Section ?? we report WMCRG results for SU(3) gauge theory with $N_f = 12$ flavors of massless

fermions in the fundamental representation.

This 12-flavor model has been studied by many groups, including Refs. [8, 20, 22, 5, 34, 19, 18, 41, 42, 4, 23, 24, 40, 16, 2, 36, 37, 17]. Using new ensembles of 12-flavor gauge configurations generated with exactly massless fermions, our improved WMCRG technique predicts a conformal IRFP where the step-scaling function vanishes. As with every method, it is essential to study the systematic effects. For WMCRG the most important systematic effects are due to the finite volume and limited number of blocking steps. While we are not able to carry out a rigorous infinite-volume extrapolation, the observed zero of the bare step-scaling function is present for all investigated lattice volumes and renormalization schemes, and agrees with the earlier MCRG results of Ref. [34]. The results of our complementary $N_f = 12$ investigations of finite-temperature phase transitions [52, 36], the Dirac eigenmode number [16, 17], and finite-size scaling [37] are also consistent with the existence of an infrared fixed point and IR conformality.

6.2   MCRG Recap?

MCRG techniques probe lattice field theories by applying RG blocking transformations that integrate out high-momentum (short-distance) modes, moving the system in the infinite-dimensional space of lattice-action couplings. In an IR-conformal system on the $m = 0$ critical surface, a renormalized trajectory runs from the perturbative gaussian FP (where the gauge coupling β is a relevant operator) to the IRFP (where β is irrelevant). Because the locations of these fixed points in the action-space depend on the renormalization scheme, each scheme corresponds to a different renormalized trajectory. The RG flow produced by the blocking steps moves the system towards and along the renormalized trajectory, from the perturbative FP to the infrared fixed point. At stronger couplings, where we would naïvely expect backward flow, there might be no ultraviolet FP to drive the RG flow along a renormalized trajectory. Except in the immediate vicinity of the IRFP, every method that attempts to determine the strong-coupling flow of the gauge coupling (including MCRG two-lattice matching) might then become meaningless.

We determine the bare step-scaling function $s_b(\beta_1)$ by matching the lattice actions $S(\beta_1, n_b)$

and $S(\beta_2, n_{b-1})$ for systems with bare couplings $\{\beta_1, \beta_2\}$ after $\{n_b, n_{b-1}\}$ blocking steps: $s_b(\beta_1) \equiv \lim_{n_b \to \infty} \beta_1 - \beta_2$ [49]. When the lattice actions are identical, all observables are identical. We use the plaquette, the three six-link loops and a planar eight-link loop to perform this matching. Using short-distance gauge observables allows us to carry out more blocking steps, down to small 2^4 or 3^4 lattices. We minimize finite-volume effects by comparing observables measured on the same blocked volume [34]. We perform the matching independently for each observable, fitting the data as a cubic function of β to smoothly interpolate between investigated values of the gauge coupling.

Our finite lattices only allow a few blocking steps, so we must optimize the procedure to reach the renormalized trajectory in as few steps as possible. In practice, we optimize by tuning some parameter so that consecutive RG blocking steps yield the same $\beta_1 - \beta_2$, which we identify as $s_b(\beta_1)$. Traditional optimization tunes the RG blocking transformation at each coupling separately, resulting in a different renormalization scheme at each bare coupling β_1: the s_b we obtain is a composite of many different discrete β functions. The Wilson flow provides a parameter that we can tune without changing the scheme.

6.3   Wilson Flow Optimized MCRG

The Wilson flow is a continuous smearing transformation [46] that removes UV fluctuations without changing the lattice scale, as shown in Fig. 6.1. In perturbation theory it is related to the $\overline{\text{MS}}$ running coupling [43], and can be used to compute a renormalized step-scaling function [26, 27].

In this work we use the Wilson flow to optimize MCRG two-lattice matching with a fixed RG blocking transformation (renormalization scheme). The Wilson flow continuously moves the system on a surface of constant lattice scale in the infinite-dimensional space of lattice-action couplings. We tune the flow time to bring the system as close as possible to the renormalized trajectory. After running the optimal amount of Wilson flow on the unblocked lattices, we then carry out the MCRG two-lattice matching. Because the renormalization scheme is fixed, we obtain a bare step-scaling function that corresponds to a unique discrete β function.

6.4   12 Flavor Results

Our WMCRG results for the 12-flavor system are obtained on gauge configurations generated with exactly massless fermions. Our lattice action uses nHYP-smeared staggered fermions as described in Ref. [18], and to run with $m = 0$ we employ anti-periodic boundary conditions in all four directions. All of our analyses are carried out at couplings weak enough to avoid the unusual strong-coupling "$\mathcal{S}^4$" phase discussed by Refs. [18, 36].

We perform three-lattice matching with volumes 6^4–12^4–24^4 and 8^4–16^4–32^4. Three-lattice matching is based on two sequential two-lattice matching steps, to minimize finite-volume effects [34]. Both two-lattice matching steps are carried out on the same final volume V_f. We denote the number of blocking steps on the largest volume by n_b, and tune the length of the initial Wilson flow by requiring that the last two blocking steps predict the same step-scaling function. Using the 8^4–16^4–32^4 data we determine the bare step-scaling function for $n_b = 3$ and $V_f = 4^4$ as well as $n_b = 4$ and $V_f = 2^4$, while the 6^4–12^4–24^4 data set is blocked to a final volume $V_f = 3^4$ ($n_b = 3$). This allows us to explore the effects of both the final volume and the number of blocking steps. We investigate three renormalization schemes by changing the HYP smearing parameters in our blocking transformation [49]: scheme 1 uses smearing parameters (0.6, 0.2, 0.2), scheme 2 uses (0.6, 0.3, 0.2) and scheme 3 uses (0.65, 0.3, 0.2).

Figs. 6.2, 6.3 and 6.4 present representative results for 12 flavors. All of the bare step-scaling functions clearly show $s_b = 0$, signalling an infrared fixed point, for every n_b, V_f and renormalization scheme. Appropriately for an IR-conformal system, the location of the fixed point is scheme dependent. We observe that the fixed point moves to stronger coupling as the HYP smearing parameters in the RG blocking transformation increase.

When we block our 8^4, 16^4 and 32^4 lattices down to a final volume $V_f = 2^4$ (corresponding to $n_b = 4$), the observables become very noisy, making matching more difficult. The problem grows worse as the HYP smearing parameters increase, and our current statistics do not allow reliable three-lattice matching for $V_f = 2^4$ in schemes 2 and 3. To resolve this issue, we are accumulating

more statistics in existing 32^4 runs, and generating additional 32^4 ensembles at more values of the gauge coupling β_F. These additional data will also improve our results for scheme 1, which we show in Fig. 6.4. Different volumes and n_b do not produce identical results in scheme 1, suggesting that the corresponding systematic effects are still non-negligible. We can estimate finite-volume effects by comparing $n_b = 3$ with $V_f = 3^4$ and $V_f = 4^4$. Systematic effects due to n_b can be estimated from $n_b = 4$ and $V_f = 2^4$, but this is difficult due to the noise in the 2^4 data. Even treating the spread in the results shown in Fig. 6.4 as a systematic uncertainty, we still obtain a clear zero in the bare step-scaling function, indicating an IR fixed point.

6.5   Summary

In this proceedings we have shown how the Wilson-flow-optimized MCRG two-lattice matching procedure proposed in Ref. [49] improves upon traditional lattice renormalization group techniques. By optimizing the flow time for a fixed RG blocking transformation, WMCRG predicts a bare step-scaling function s_b that corresponds to a unique discrete β function. Applying WMCRG to new 12-flavor ensembles generated with exactly massless fermions, we observe an infrared fixed point in s_b. The fixed point is present for all investigated lattice volumes, number of blocking steps and renormalization schemes, even after accounting for systematic effects indicated by Fig. 6.4. This result reinforces the IR-conformal interpretation of our complementary $N_f = 12$ studies of phase transitions [52, 36], the Dirac eigenmode number [16, 17], and finite-size scaling [37].

6.6   copied from first paper

6.6.1   Wilson-flowed MCRG

As an alternative to optimizing the RG blocking transformation, and thus changing the renormalization scheme at each coupling β_F, here we propose to use the Wilson flow to move the lattice system as close as possible to the renormalized trajectory of a fixed renormalization scheme.

The Wilson flow is a continuous smearing transformation [46] that can be related to the

$\overline{\text{MS}}$ running coupling in perturbation theory [43]. Refs. [26, 27] recently used the Wilson flow to compute a renormalized step-scaling function in a way similar to Schrödinger functional methods. While this approach appears very promising, it is based on perturbative relations that are only fully reliable at weak coupling. Here we do not use this perturbative connection, instead applying the Wilson flow as a continuous smearing that removes UV fluctuations. The Wilson flow moves the system along a surface of constant lattice scale in the infinite-dimensional action-space; it is not a renormalization group transformation and does not change the IR properties of the system.

Our goal is to use a one-parameter Wilson flow transformation to move the lattice system as close as possible to the renormalized trajectory of our fixed RG blocking transformation. We proceed by carrying out two-lattice matching after applying the Wilson flow for a flow time t_f on all lattice volumes. (The Wilson flow is run only on the unblocked lattices, not in between RG blocking steps.) As above, since we can block our lattices only a few times, we must optimize t_f by requiring that consecutive RG blocking steps yield the same $\Delta\beta_F$, as shown in the right panel of Fig. 4.5. As for traditional MCRG, increasing the number of blocking steps reduces the dependence on the optimization parameter; in the limit $n_b \to \infty$, our results would be independent of t_f.

With Wilson-flowed MCRG we can efficiently determine bare step-scaling functions that correspond to unique RG β functions. This new capability opens up interesting directions for future studies. By comparing different β functions around the perturbative gaussian FP, we can study scaling violations in the lattice system. In IR-conformal systems, we can investigate the scheme-dependence of the β function near the IRFP, an issue explored in perturbation theory by Ref. [51].

6.6.2   Wilson-flowed MCRG

Fig. 6.5 presents our results for the bare step-scaling function s_b from Wilson-flowed MCRG two-lattice matching. We continue using two sequential HYP smearings in our RG blocking transformation, but now fix the smearing parameters to $(0.5, 0.2, 0.2)$. We again use $24^3 \times 48$ and $12^3 \times 24$ lattices with fermion masses $m = 0.0025$ and $m = 0.01$, respectively, and determine uncertainties

in the same way as described in the previous subsection. In this preliminary study we don't yet employ the volume-corrected optimization discussed in Ref. [34]; for our lattice volumes, Ref. [34] found that neglecting this finite-volume correction introduces only a small additional error. Our final results will use the appropriate optimization, and will also present further consistency checks from larger lattices up to $32^3 \times 64$.

While our results in Fig. 6.5 from combining the Wilson flow with MCRG two-lattice matching are qualitatively similar to the results of the traditional approach in Fig. **??**, we can now identify the bare step-scaling function s_b with a unique discrete β function. In the renormalization scheme defined by our RG blocking transformation with HYP-smearing parameters $(0.5, 0.2, 0.2)$, we find a 12-flavor IRFP at $5 < \beta_F^\star \lesssim 6$. Although $\beta_F^\star$ is scheme-dependent, the existence of this IRFP is physical. We are currently exploring other choices of renormalization schemes, to non-perturbatively investigate the scheme-dependence of the β function near the IRFP [51]. At weaker couplings, we will also attempt to use similar explorations to study scaling violations in our lattice systems.
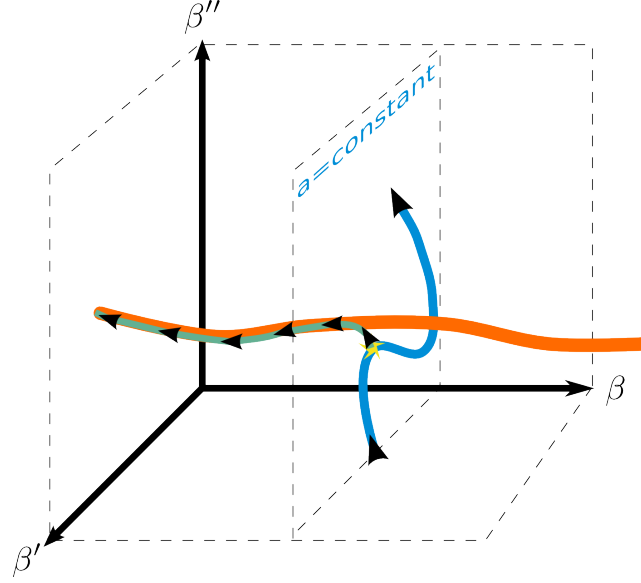
Figure 6.1: The Wilson flow (blue) moves systems on a surface of constant lattice scale a (normal to the orange renormalized trajectory) in the infinite-dimensional coupling space. Wilson-flow-optimized MCRG tunes the flow time to bring the system close to the renormalized trajectory (yellow star), so that MCRG blocking (green) quickly reaches the renormalized trajectory.
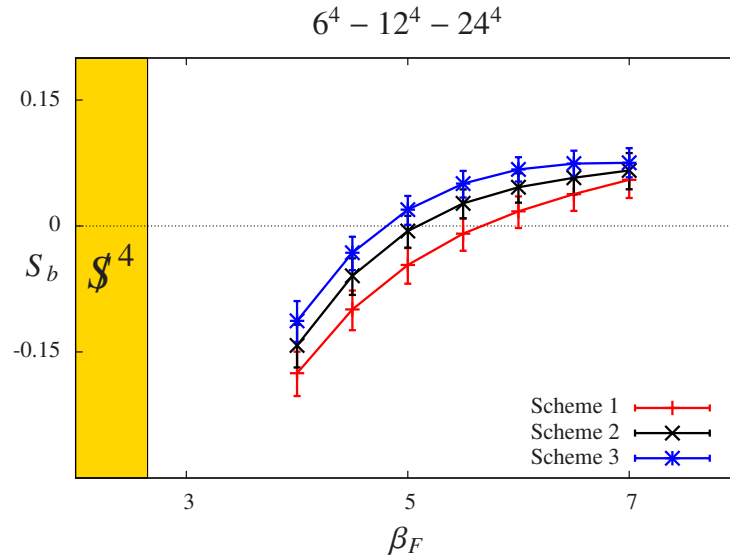

Figure 6.2: The bare step-scaling function s_b predicted by three-lattice matching with 6^4, 12^4 and 24^4 lattices blocked down to 3^4, comparing three different renormalization schemes. The error bars come from the standard deviation of predictions using the different observables discussed in Section ??.
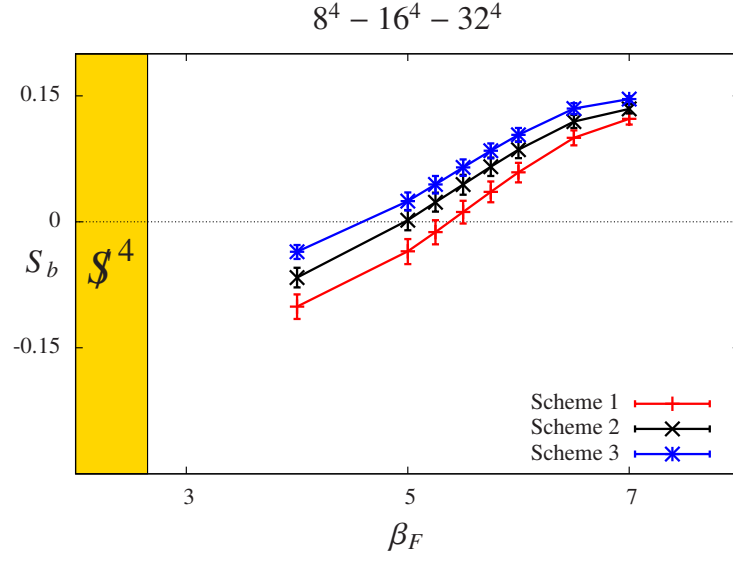
Figure 6.3: As in Fig. 6.2, the bare step-scaling function s_b for three different renormalization schemes from three-lattice matching, now using 8^4, 16^4 and 32^4 lattices blocked down to 4^4.
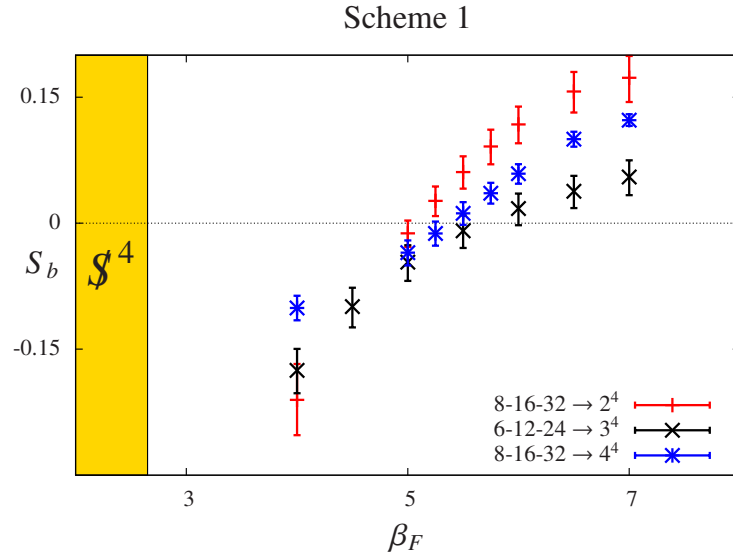

Figure 6.4: The bare step-scaling function s_b for scheme 1, comparing three-lattice matching using different volumes: 6^4, 12^4 and 24^4 lattices blocked down to 3^4 (black $\times$s) as well as 8^4, 16^4 and 32^4 lattices blocked down to 4^4 (blue bursts) and 2^4 (red crosses).
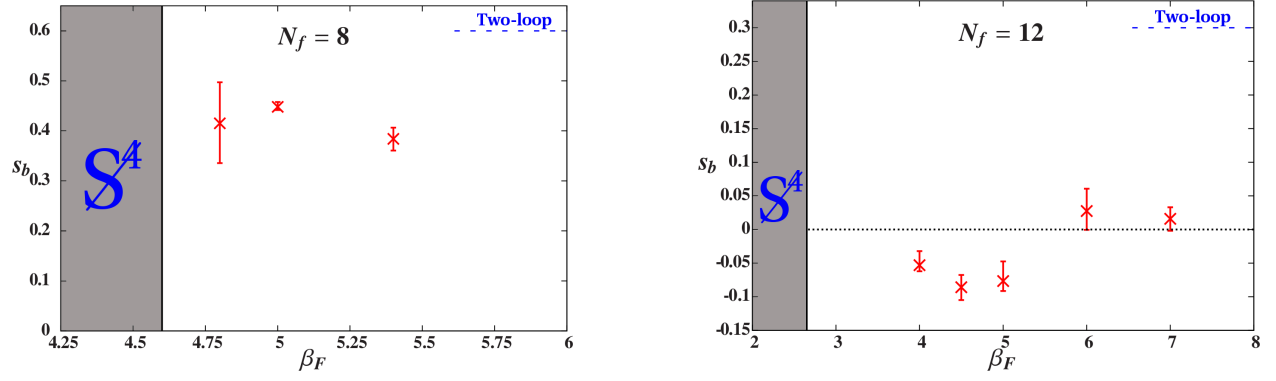
Figure 6.5: Preliminary results for the bare step-scaling function s_b from Wilson-flowed MCRG two-lattice matching with $24^3 \times 48$ and $12^3 \times 24$ lattice volumes, for $N_f = 8$ (left) and $N_f = 12$ (right) with fixed HYP-smearing parameters $(0.5, 0.2, 0.2)$. The blue dashed lines are perturbative predictions for asymptotically weak coupling.

Chapter 7

Conclusion

Truly it is an exciting time in particle physics. For almost two decades since the discovery of the top quark no new fundamental particles were discovered in collider experiments. After a long wait the Higgs particle has been discovered, completing the standard model. Although the standard model is complete we know it must be an effective theory and our knowledge of the Higgs mass puts constraints on beyond standard model physics.

Many proposals for beyond standard model physics, including technicolor, are strongly coupled theories and thus inherently nonperturbative. Since the lattice offers the only controlled means of studying non perturbative field theories in a controlled manner, it is natural that strongly coupled beyond standard model is an active area of lattice research. Studying BSM physics on the lattices has created many new challenges for the lattice community to solve. Unlike QCD, we don't know the answer to most questions before hand, and there are no experimental results to compare lattice results with. Furthermore just because a technique is successful when studying QCD does not mean that it will work just as well in systems that are very different from QCD. Accordingly it is important to approach each theory studied carefully and with an open mind. Only when several methods converge on the same result can that result be trusted. Additionally since there is more than one way to put a continuum theory on the lattice, it is important to understand the effect of the lattice action and lattice artifacts.

The lattice search for viable technicolor theories has focused on exploring gauge theories with $SU(N_c)$ colors and N_f fermions in some representation R. By changing these parameters

generates theories with dramatically different behavior. Theories with a small number of fermionic flavors in a lower representation behave similarly to QCD. If more fermionic degrees of freedom are added the theory develops and infrared fixed point. If enough degrees of freedom are added the theory will loose asymptotic freedom. The location of the conformal window in the parameter space N_c, N_f, and R is fundamentally a question of strong dynamics. Perturbative and quasi pertrubative calculations exist for the bounds of the conformal window but they can only serve as a guide to locate interesting theories for numerical studies.

Ultimately we are interested in the behavior of theories that may exhibit a slowly running coupling. This behavior, also called walking, may exist just below the conformal window. In a walking theory γ_m should be of order 1. Such a theory is strongly favored by limits on flavor changing neutral currents in the SM. To date a viable walking theory has not yet been found.

Many groups, including our own have explored the conformal window with several goals in mind. First understand the extent of the conformal window. Second improve lattice techniques in conformal systems. Third explore the bottom of the conformal window for walking behavior.

In this thesis I have discussed three methods that can be used to understand the β function. These methods are general and work for confining and conformal systems, they have the benefit that distinguishing between the two is straight forward. I first discussed MCRG and presented results for $SU(3)$ gauge theory with $N_f = 8$ and $N_f = 12$. Our results were consistent with the 12 flavor theory exhibiting an IRFP. The 8 flavor theory did not show a fixed point and appeared to be chirally broken and confining.

Next I introduced the gradient flow step scaling and showed results for $SU(3)$ gauge theory with $N_f = 4$ and N_f=12. The 4 flavor results were simply to show that our improvement works in a theory we know to be chirally broken. They also serve as a contrast to the 12 flavor results which clearly indicate an IRFP. Another group has recently applied this technique, with our improvement, to $SU(3)$ gauge theory with 8 flavors [] their results show that while the theory runs slowly they can not locate an IRFP.

Finally I introduced an improvement to MCRG that uses the Wilson flow as an optimization.

We call this technique Wilson Flow MCRG or WMCRG. WMCRG is like MCRG in that we are calculating the discrete step scaling function. By using the Wilson Flow as an optimization we are able to probe a single renormalized trajectory. Results from WMCRG for $SU(3)$ gauge theory of 12 flavors of fermions in the fundamental representation shows very clear evidence of a fixed point.

One of the benefits of these three techniques is that they are computationally inexpensive and do not require specific lattice dimensions or special boundary conditions. That is the lattices that we use for these step scaling studies are able to be used in other studies as well. Our group has been involved with several other analysis.

Finite temperature phase transitions

eigenmodes

fininte size scaling

For several years the IR physics of $SU(3)$ gauge theory with 12 flavors of fermions in the fundamental representation was a topic of debate. Several early papers [] A consensus has emerged that the theory is indeed conformal. This consensus is a result of improvements in our understanding of quantum field theories as well as implements in lattice techniques used to study those quantum field theories.

Bibliography

[1] Yasumichi Aoki, Tatsumi Aoyama, Masafumi Kurachi, Toshihide Maskawa, Kohtaroh Miura, Kei-ichi Nagai, Hiroshi Ohki, Enrico Rinaldi, Akihiro Shibata, Koichi Yamawaki, and Takeshi Yamazaki. Light composite scalar in eight-flavor QCD on the lattice. 2014.

[2] Yasumichi Aoki, Tatsumi Aoyama, Masafumi Kurachi, Toshihide Maskawa, Kei-ichi Nagai, Hiroshi Ohki, Enrico Rinaldi, Akihiro Shibata, Koichi Yamawaki, and Takeshi Yamazaki. 2013.

[3] Yasumichi Aoki, Tatsumi Aoyama, Masafumi Kurachi, Toshihide Maskawa, Kei-ichi Nagai, Hiroshi Ohki, Enrico Rinaldi, Akihiro Shibata, Koichi Yamawaki, and Takeshi Yamazaki. Light composite scalar in twelve-flavor QCD on the lattice. Phys. Rev. Lett., 111:162001, 2013.

[4] Yasumichi Aoki, Tatsumi Aoyama, Masafumi Kurachi, Toshihide Maskawa, Kei-ichi Nagai, Hiroshi Ohki, Akihiro Shibata, Koichi Yamawaki, and Takeshi Yamazaki. Phys. Rev., D86:054506, 2012.

[5] T. Appelquist, G. T. Fleming, M. F. Lin, E. T. Neil, and D. Schaich. Phys. Rev., D84:054501, 2011.

[6] Thomas Appelquist, Richard Brower, Simon Catterall, George Fleming, Joel Giedt, Anna Hasenfratz, Julius Kuti, Ethan Neil, and David Schaich. Lattice Gauge Theories at the Energy Frontier. 2013.

[7] Thomas Appelquist, George T. Fleming, and Ethan T. Neil. Lattice study of the conformal window in QCD-like theories. Phys. Rev. Lett., 100:171607, 2008.

[8] Thomas Appelquist, George T. Fleming, and Ethan T. Neil. Phys. Rev., D79:076010, 2009.

[9] Janos Balog, Ferenc Niedermayer, and Peter Weisz. Logarithmic corrections to O(a**2) lattice artifacts. Phys. Lett., B676:188–192, 2009.

[10] Janos Balog, Ferenc Niedermayer, and Peter Weisz. The Puzzle of apparent linear lattice artifacts in the 2d non-linear sigma-model and Symanzik's solution. Nucl. Phys., B824:563–615, 2010.

[11] Tom Banks and A. Zaks. On the Phase Structure of Vector-Like Gauge Theories with Massless Fermions. Nucl. Phys., B196:189, 1982.

[12] Szabolcs Borsanyi, Stephan Durr, Zoltan Fodor, Christian Hoelbling, Sandor D. Katz, S. Krieg, T. Kurth, L. Lellouch, T. Lippert, C. McNeile, and K. K. Szabo. JHEP, 1209:010, 2012.

[13] William E. Caswell. Asymptotic Behavior of Nonabelian Gauge Theories to Two Loop Order. Phys. Rev. Lett., 33:244, 1974.

[14] Anqi Cheng, Anna Hasenfratz, Yuzhi Liu, Gregory Petropoulos, and David Schaich. Finite size scaling of conformal theories in the presence of a near-marginal operator. 2013.

[15] Anqi Cheng, Anna Hasenfratz, Yuzhi Liu, Gregory Petropoulos, and David Schaich. Step scaling studies using the gradient flow running coupling. 2014, in preparation.

[16] Anqi Cheng, Anna Hasenfratz, Gregory Petropoulos, and David Schaich. JHEP, 1307:061, 2013.

[17] Anqi Cheng, Anna Hasenfratz, Gregory Petropoulos, and David Schaich. PoS, LATTICE 2013:088, 2013.

[18] Anqi Cheng, Anna Hasenfratz, and David Schaich. Phys. Rev., D85:094509, 2012.

[19] Thomas DeGrand. Phys. Rev., D84:116901, 2011.

[20] A. Deuzeman, M. P. Lombardo, and E. Pallante. Phys. Rev., D82:074503, 2010.

[21] Albert Deuzeman, Maria Paola Lombardo, Tiago Nunes da Silva, and Elisabetta Pallante. 2012.

[22] Zoltan Fodor, Kieran Holland, Julius Kuti, Daniel Nogradi, and Chris Schroeder. Phys. Lett., B703:348–358, 2011.

[23] Zoltan Fodor, Kieran Holland, Julius Kuti, Daniel Nogradi, Chris Schroeder, and Chik Him Wong. PoS, Lattice 2012:025, 2012.

[24] Zoltan Fodor, Kieran Holland, Julius Kuti, Daniel Nogradi, Chris Schroeder, and Chik Him Wong. 2012.

[25] Zoltan Fodor, Kieran Holland, Julius Kuti, Daniel Nogradi, Chris Schroeder, and Chik Him Wong. Can the nearly conformal sextet gauge model hide the Higgs impostor? Phys. Lett., B718:657–666, 2012.

[26] Zoltan Fodor, Kieran Holland, Julius Kuti, Daniel Nogradi, and Chik Him Wong. 2012.

[27] Zoltan Fodor, Kieran Holland, Julius Kuti, Daniel Nogradi, and Chik Him Wong. PoS, Lattice 2012:050, 2012.

[28] Zoltan Fodor, Kieran Holland, Julius Kuti, Daniel Nogradi, and Chik Him Wong. Can a light Higgs impostor hide in composite gauge models? PoS, LATTICE 2013:062, 2014.

[29] Patrick Fritzsch and Alberto Ramos. The gradient flow coupling in the Schrdinger Functional. JHEP, 1310:008, 2013.

[30] Joel Giedt. PoS, Lattice 2012:006, 2012.

[31] Joel Giedt. Lattice gauge theory and physics beyond the standard model. PoS, Lattice 2012:006, 2012.

[32] Anna Hasenfratz. Conformal or Walking? Monte Carlo renormalization group studies of SU(3) gauge models with fundamental fermions. Phys. Rev., D82:014506, 2010.

[33] Anna Hasenfratz. PoS, Lattice 2011:065, 2011.

[34] Anna Hasenfratz. Phys. Rev. Lett., 108:061601, 2012.

[35] Anna Hasenfratz, Anqi Cheng, Gregory Petropoulos, and David Schaich. PoS, Lattice 2012:034, 2012.

[36] Anna Hasenfratz, Anqi Cheng, Gregory Petropoulos, and David Schaich. 2013.

[37] Anna Hasenfratz, Anqi Cheng, Gregory Petropoulos, and David Schaich. PoS, LATTICE 2013:075, 2013.

[38] Anna Hasenfratz, Roland Hoffmann, and Stefan Schaefer. Hypercubic smeared links for dynamical fermions. JHEP, 0705:029, 2007.

[39] Anna Hasenfratz and Francesco Knechtli. Flavor symmetry and the static potential with hypercubic blocking. Phys. Rev., D64:034504, 2001.

[40] Etsuko Itou. PTEP, 2013:083B01, 2013.

[41] Xiao-Yong Jin and Robert D. Mawhinney. PoS, Lattice 2011:066, 2012.

[42] C.-J. David Lin, Kenji Ogawa, Hiroshi Ohki, and Eigo Shintani. JHEP, 1208:096, 2012.

[43] Martin Luscher. JHEP, 1008:071, 2010.

[44] Martin Luscher. Trivializing maps, the Wilson flow and the HMC algorithm. Commun. Math. Phys., 293:899–919, 2010.

[45] Shinya Matsuzaki and Koichi Yamawaki. Holographic techni-dilaton at 125 GeV. Phys. Rev., D86:115004, 2012.

[46] R. Narayanan and H. Neuberger. JHEP, 0603:064, 2006.

[47] Ethan T. Neil. Exploring Models for New Physics on the Lattice. PoS, Lattice 2011:009, 2011.

[48] Paula Perez-Rubio and Stefan Sint. Non-perturbative running of the coupling from four flavour lattice QCD with staggered quarks. PoS, Lattice 2010:236, 2010.

[49] Gregory Petropoulos, Anqi Cheng, Anna Hasenfratz, and David Schaich. PoS, Lattice 2012:051, 2012.

[50] Gregory Petropoulos, Anqi Cheng, Anna Hasenfratz, and David Schaich. Improved Lattice Renormalization Group Techniques. PoS, LATTICE 2013:079, 2013.

[51] Thomas A. Ryttov and Robert Shrock. Phys.Rev., D86:085005, 2012.

[52] David Schaich, Anqi Cheng, Anna Hasenfratz, and Gregory Petropoulos. PoS, Lattice 2012:028, 2012.

[53] Rainer Sommer. Scale setting in lattice QCD. <u>PoS</u>, LATTICE 2013:015, 2014.

[54] Fatih Tekin, Rainer Sommer, and Ulli Wolff. The Running coupling of QCD with four flavors. <u>Nucl. Phys.</u>, B840:114–128, 2010.

List of Abbreviations

There are several abbreviations and acronyms used throughout this thesis. I try my best to define terminology when it first appears in the text. However, there are likely places that I have overlooked. Furthermore it can be confusing keeping track of acronyms and abbreviations defined several chapters ago. I have compiled a list here for quick reference.